

1 **A conserved fungal Knr4/Smi1 protein is vital**
2 **for maintaining cell wall integrity and host**
3 **plant pathogenesis**

4 **Erika Kroll^{1,2}, Carlos Bayon¹, Jason Rudd¹, Victoria Armer¹, Anjana Magaji-**
5 **Umashankar¹, Ryan Ames³, Martin Urban¹, Neil A. Brown², and Kim Hammond-**
6 **Kosack^{1,*}**

7 Author addresses: ¹Strategic Area: Protecting Crops and the Environment, Rothamsted
8 Research, Harpenden, AL5 2JQ, UK

9 ²Department of Life Sciences, University of Bath, Bath, BA2 7AY, UK

10 ³Biosciences and Living Systems Institute, University of Exeter, EX4 4PY, Exeter, UK

11 **Corresponding authors:**

12 *To whom correspondence should be addressed. Tel: +44 1582 938240. Email:

13 kim.hammond-kosack@rothamsted.ac.uk

14

15 Abstract

16 Filamentous plant pathogenic fungi pose significant threats to global food security,
17 particularly through diseases like Fusarium Head Blight (FHB) and Septoria Tritici Blotch
18 (STB) which affects cereals. With mounting challenges in fungal control and increasing
19 restrictions on fungicide use due to environmental concerns, there is an urgent need for
20 innovative control strategies. Here, we present a comprehensive analysis of the stage-
21 specific infection process of *Fusarium graminearum* in wheat spikes by generating a dual
22 weighted gene co-expression network (WGCN). Notably, the network contained a
23 mycotoxin-enriched fungal module that exhibited a significant correlation with a detoxification
24 gene-enriched wheat module. This correlation in gene expression was validated through
25 quantitative PCR.
26 By examining a fungal module with genes highly expressed during early symptomless
27 infection, we identified a gene encoding FgKnr4, a protein containing a Knr4/Smi1
28 disordered domain. Through comprehensive analysis, we confirmed the pivotal role of
29 FgKnr4 in various biological processes, including morphogenesis, growth, cell wall stress
30 tolerance, and pathogenicity. Further studies confirmed the observed phenotypes are
31 partially due to the involvement of FgKnr4 in regulating the fungal cell wall integrity pathway
32 by modulating the phosphorylation of the MAP-kinase MGV1. Orthologues of *FgKnr4* are
33 widespread across the fungal kingdom but are absent in other Eukaryotes, suggesting the
34 protein has potential as a promising intervention target. Encouragingly, the restricted growth
35 and highly reduced virulence phenotypes observed for $\Delta Fgknr4$ were replicated upon
36 deletion of the orthologous gene in the wheat fungal pathogen *Zymoseptoria tritici*. Overall,
37 this study demonstrates the utility of an integrated network-level analytical approach to
38 pinpoint genes of high interest to pathogenesis and disease control.

39 **Keywords: *Fusarium graminearum*, *Zymoseptoria tritici*, Weighted Gene Co-**
40 **expression Network (WGCNA), dual host-pathogen transcriptomics, cell wall stress,**
41 **MAP-kinase signalling, fungal specific gene family, fungal virulence.**

42

43

Introduction

44 The wheat crop (*Triticum* species) plays a crucial role in global food security, contributing
45 about 20% of dietary calories and protein worldwide (Saldivar, 2016), while also supplying
46 essential nutrients and bioactive food components (Shewry and Hey, 2015). Pathogen and
47 pest burden substantially contribute to wheat losses globally, accounting for ~21.5% of
48 wheat losses annually (Savary et al., 2019). Of these, the five highest global contributors to
49 wheat yield and quality losses are all fungal diseases and include Fusarium Head Blight
50 disease (FHB) and Septoria tritici blotch disease (STB), which account for 2.85% and 2.44%
51 of wheat losses, respectively (Savary et al., 2019).

52 FHB is a mycotoxicogenic pre-harvest fungal disease of most cereals, caused by different
53 *Fusaria* within the *Fusarium sambucinum* species complex that is increasingly prevalent in
54 most cereal growing regions globally (O'Donnell et al., 2000; Kanja et al., 2021; Johns et al.,
55 2022; Armer et al., 2024). Floral Infections lead to contamination of grain with mycotoxins
56 that are subject to strict legal limits in different global regions (European Commission, 2006;
57 EFSA, 2017; AHDB, 2023). Despite ongoing endeavours to manage FHB, mycotoxin
58 contamination continues to significantly impact the economies of cereal and livestock
59 producers, as well as the food, drink, and feed industries (Latham et al., 2023). The B-type
60 sesquiterpenoid deoxynivalenol (DON) is the most common FHB mycotoxin in European
61 food and feed wheat (Johns et al., 2022). The globally predominant DON producing species
62 is *Fusarium graminearum* (O'Donnell et al., 2000). During wheat spike colonisation, *F.*
63 *graminearum* undergoes a biphasic mode of infection. Initially, the fungus evades the host
64 immune response by growing between cells, causing no visible symptoms for ~3 days. This

65 is followed by an extended symptomatic stage marked by wheat tissue bleaching and
66 reduced grain development behind the advancing hyphal front (Brown et al., 2010, 2011).
67 STB disease on wheat leaves is caused by the fungus *Zymoseptoria tritici*. This fungus has
68 an extended symptomless stage of infection ~9 days, followed by a switch to symptomatic
69 disease (Goodwin et al., 2011; Steinberg, 2015). However, unlike *F. graminearum*, *Z. tritici*
70 colonisation is strictly confined to the sub-stomatal cavities and apoplastic spaces, without
71 ever invading host cells (Kema et al., 1996). Both pathogens are currently managed using
72 semi effective sources of host resistance mediated by major genes or QTLs (Brown et al.,
73 2015; Bai et al., 2018; Buerstmayr et al., 2020) as well as fungicide applications (Fones and
74 Gurr, 2015; Torriani et al., 2015; Buerstmayr et al., 2020; Kanja et al., 2021). But effective
75 control faces escalating issues caused by fungicide resistance (Estep et al., 2015; Lucas et
76 al., 2015; McDonald et al., 2019; de Chaves et al., 2022). There is a critical need to develop
77 new methods to combat these and other wheat fungal pathogens.

78 Understanding the genetic and molecular mechanisms driving host infection in numerous
79 interaction types continues to be a major goal of the international molecular plant pathology
80 community (Nelson, 2020; Jeger et al., 2021). Gene expression data can be organised into
81 co-expression networks, which group genes based on shared co-expression patterns.
82 Network representations are advantageous because these present biological data on a
83 systems-wide level, clustering genes in modules representative of specific stages or
84 functions. This modelling can be achieved using the weighted gene co-expression network
85 analysis (WGCNA) framework (Langfelder and Horvath, 2008). WGCNA has been
86 repeatedly applied to analyse fungal gene expression data. For instance, this approach has
87 been employed to identify effectors in *Magnaporthe oryzae* (Yan et al., 2023), shared genes
88 during *Fusarium oxysporum* infection across multiple hosts (Cai et al., 2022), and virulence
89 genes of *Colletotrichum siamense* (Liu et al., 2023). Although WGCNA has been used to
90 study wheat host responses to *F. graminearum* infection (Kugler et al., 2013; Pan et al.,
91 2018) and responses of *F. graminearum* under *in vitro* stress (L. Zhang et al., 2022; Park et

92 al., 2023), there has been no study of wheat-*F. graminearum* co-expression profiles during
93 infection.

94 To gain deeper insight on the expression patterns of genes during the different stages of the
95 *F. graminearum* infection the WGCNA framework was used to generate a fungal
96 pathogen/wheat dual co-expression network. Significantly, this framework can facilitate the
97 correlation of both fungal and host plant expression (Mateus et al., 2019). Within this
98 approach, genes are grouped into modules based on shared co-expression patterns
99 separately for the pathogen and the host. Modules are then correlated between the
100 pathogen and host networks to predict shared expression dynamics. In this study, correlated
101 expression between a mycotoxin gene-enriched fungal module and a detoxification gene-
102 enriched wheat module, validated the host-pathogen network. The study then focused on the
103 unique fungal module F16, characterised by high expression levels during the earliest
104 symptomless infection stage, and led to the discovery of *FgKnr4*. A subsequent
105 comprehensive experimental analysis revealed the pivotal role of *FgKnr4* in various
106 biological processes, including morphogenesis, growth, cell wall stress tolerance, and
107 virulence in *F. graminearum*. The *Knr4* gene is not restricted to *F. graminearum* but is
108 distributed widely across the fungal kingdom and is absent in other Eukaryotes. The various
109 mutant phenotypes observed in the *F. graminearum* $\Delta Fgknr4$ strain were replicated upon
110 deletion of the orthologous gene in the wheat pathogen *Z. tritici*. Overall, this study highlights
111 the value of using network analyses to model spatio-temporal pathogen-host interactions
112 and to identify novel conserved genes associated with virulence.

113

114 **Results**

115 **Generation of a dual *F. graminearum*-wheat co-expression**

116 **network**

117 *F. graminearum* floral infections can be divided into symptomatic or symptomless stages of
118 infection. Disease spread through the rachis internodes (RI) can be further broken down to
119 four different key stages of infection. Namely early symptomless (RI7-8), late symptomless
120 (RI5-6), early symptomatic (RI3-4), and late symptomatic (RI1-2) infection (**Figure 1A**). A
121 spatio-temporal transcriptomics dataset of *F. graminearum* floral infection of the susceptible
122 wheat cultivar Bobwhite, which distinguishes between these key distinct stages, was
123 previously generated (Dilks et al., 2019). This dataset also included spikelet tissue (SP)
124 sampled at 3 (early symptomatic) and 7 days post-infection (dpi) (late symptomatic). The
125 WGCNA framework (Zhang and Horvath, 2005; Langfelder and Horvath, 2008) was used to
126 construct a dual co-expression network to model fungal pathogen/crop interaction in wheat
127 using this dataset.

128 Normalised counts were used to generate two distinct networks: one for *F. graminearum* and
129 another for *T. aestivum*. The *F. graminearum* network consisted of 10,189 genes organised
130 into 18 modules (with 2629 – 60 genes per module), while the *T. aestivum* network consisted
131 of 47,458 genes distributed among 25 modules (with 23063 – 83 genes per module) (**Figure**
132 **2 – figure supplement 1, Supplementary File 1**). Both networks met scale free model
133 criteria at their selected soft thresholding power (**Figure 2 – figure supplement 2 A-B**). The
134 examination of module quality statistics found that each module within both networks were of
135 a high quality (Z-Summary > 10), with the exception of F16 (Z-Summary = 9.67), which still
136 markedly surpasses the minimum Z-Summary score of > 2 (Langfelder et al., 2011) (**Figure**
137 **2 – figure supplement 2C**). This indicates a substantial preservation of modules compared
138 to a random selection of all network genes. Additionally, preservation statistic calculations
139 confirmed that all modules maintain preservation (Z-summary > 2) across both networks with
140 all modules of the wheat network and the majority of the fungal modules (11/18) having
141 strong preservation (Z-summary > 10) (**Figure 2 – figure supplement 2D**). These findings
142 suggest a consistent preservation of within-network topology across modules (Langfelder et
143 al., 2011). For each module, a single summarised expression pattern, the eigengene value,

144 was calculated. The fungal and wheat modules were correlated by their eigengene
145 expression values, and modules displaying significant correlation ($p \geq 0.001$) formed the
146 dual co-expression network (**Figure 2A**).
147 To gain insight into the function of individual modules, a Gene Ontology (GO) enrichment
148 analysis was performed for both network sets (**Figure 2D-E, Figure 2 – figure supplement**
149 **1**). To confirm these enrichment patterns were not due to chance, a random network was
150 generated for both the fungal and wheat datasets. No significant enrichment was found for
151 the random wheat network and fungal network.
152 Among the eight wheat modules within the dual co-expression network, five of them were
153 significantly enriched for disease resistance genes (TO:0000112, $p \geq 0.05$) and one was
154 specifically enriched for wheat stripe rust resistance genes (TO:0020055) (**Figure 2E**),
155 suggesting the wheat modules in the network are needed for plant defence. One of these
156 wheat modules, W12, was significantly enriched in the GO terms detoxification
157 (GO:0098754; $p = 7.13 \times 10^{-7}$) and response to toxic substances (GO:0009636; $p = 2.11 \times$
158 10^{-6}). This module was correlated to the fungal module F12, which was enriched in genes
159 belonging to the trichothecene biosynthesis (*TRI*) gene cluster ($p = 1.92 \times 10^{-4}$) and for the
160 GO term terpenoid biosynthesis (GO:0016114 ; $p = 0.00085$) (**Figure 2D, Table 1**). Notably,
161 the module F12 was most highly expressed in the late symptomless stage of infection.
162 Expression of this module then rapidly decreases during the symptomatic stages of infection.
163 Module F12 therefore appears to be positioned specifically at the transition between the late
164 symptomless stage and the early symptomatic stage. The production of the DON mycotoxin
165 is essential for the transition to the extensive symptomatic stage (Cuzick et al., 2008; Jansen
166 et al., 2005). DON inhibits protein translation, which then eventually leads to cell death and
167 the bleached phenotype distinctive of symptomatic *F. graminearum* infection (Desmond et
168 al., 2008; Arunachalam and Doohan, 2013). High expression of module F12 in the
169 symptomless stage is also supported by previous data which found that genes involved in
170 mycotoxin biosynthesis are highly expressed in symptomless wheat tissue (Brown et al.,

171 2017). The correlation with the wheat module W12 therefore implies that detoxification
172 genes in the module are being expressed in response to production of fungal mycotoxins.

173 Interestingly, the fungal module F10 contains genes that are highly expressed in the earliest
174 and latest stages of *F. graminearum* infection, but not intermediate stages (**Figure 4**). The
175 fungal module F10 includes the Killer toxin 4 genes (*KP4L*) -1, -2, and -3. These genes also
176 have some of the highest module membership scores (>0.90) within the module. The *KP4L*
177 genes are necessary for virulence and expressed during both self and non-self interactions
178 (**Table 1**). It is suggested that KPL4 proteins provide *F. graminearum* with a competitive
179 advantage when occupying new niches (Vicente et al., 2022), which would explain their
180 expression during the earliest stage of infection. High expression during late infection may
181 be necessary for intraspecific interactions, when the fungus is coordinating growth at a high
182 fungal density.

183 The stress-responsive mitogen-activated protein kinase *FgOS-2* is a key regulator in *F.*
184 *graminearum* and acts upstream of the ATF/CREB-activating transcription factor *FgAtf-1*
185 (**Table 1**). Both *FgOS-2* and *FgAtf-1* cluster in module F10. These proteins are involved in
186 broad functions, including secondary metabolite production, sexual reproduction, and stress
187 tolerance (Nguyen et al., 2013). Module F10 also contains two hydrophobin genes, *FgHyd3*
188 and *FgHyd5*. *FgHyd3* is necessary for attachment to hydrophobic surfaces, while both genes
189 are necessary for the production of aerial mycelia (**Table 1**). These genes are likely to play a
190 crucial role during early infection for surface attachment and are possibly expressed again
191 during the late stage of infection to facilitate the production of aerial mycelia.

192 The fungal module F10 is correlated with the wheat module W06 ($R = 0.85, p = 6 \times 10^{-6}$),
193 which is enriched in protein catabolism (GO:0010498; $p = 1.60 \times 10^{-19}$) and autophagy
194 (GO:0006914; $p = 2.31 \times 10^{-4}$) (**Table 1**). Autophagy plays a dual role in plant immunity
195 where it is involved in immune signalling and programmed cell death to restrict pathogen
196 spread, but also in response to pathogen induced necrotic cell death (Sertsuvalkul et al.,
197 2022). Therefore, it is likely these genes are expressed during early infection as an

198 immediate immune response and then expressed again in highly colonised tissue for late-
199 stage necrotrophic damage control.

200

201 **Wheat genes in module W12 are expressed in response to**
202 **DON production**

203 To validate the correlation between modules F12 and W12 (**Figure 3A**), expression of wheat
204 genes in the detoxification module W12 in response to *F. graminearum* infection without
205 DON was examined. This was achieved by inoculating wheat plants with either the wild-type
206 *F. graminearum* reference strain PH-1, or the DON deficient $\Delta Fgtri5$ mutant strain generated
207 in the PH-1 background. Expression of three wheat genes was studied, including two
208 phenylalanine ammonia-lyases (*PAL1* and *2*; *TraesCS4A02G401300* and
209 *TraesCS2D02G377200*) which were annotated with the term disease resistance
210 (TO:0000112), and a predicted transmembrane exporter, detoxification gene 16 (*DTX16*;
211 *TraesCS5B02G371100*).

212 The first two rachis internodes below the point of inoculation (POI) were sampled at 3 days
213 post inoculation (dpi). Levels of *FgActin* cDNA were not significantly different between
214 treatments (**Figure 3B**). Expression of the three wheat genes from module W12 was
215 significantly lower in the $\Delta Fgtri5$ infected samples relative to wild-type infection (**Figure 3C**).
216 This indicates that expression of genes in module W12 is correlated with DON production,
217 thereby supporting the correlated co-expression patterns observed between modules of the
218 two networks.

219 **Dual co-expression networks as a tool to identify key**
220 **genes necessary for virulence**

221 To pinpoint *F. graminearum* genes that are necessary for virulence, the stage specific
222 expression patterns of each module was examined (**Figure 4, Figure 4 – figure**
223 **supplement 1**). The module F16 is uniquely highly expressed during the earliest stages of
224 infection, with markedly decreased expression at all the other stages of infection. This
225 module is highly correlated to two wheat modules. These are W01 ($R = 0.91$; $p = 5 \times 10^{-7}$)
226 and W05 ($R = 0.85$, $p = 2 \times 10^{-5}$). W01 is the largest wheat module and is enriched for
227 defence response genes (GO:0006952; $p = 3.60 \times 10^{-88}$), but also maintenance genes which
228 include photosynthesis (GO:0015979; $p = 4.59 \times 10^{-29}$) and RNA modification (GO:0009451;
229 $p = 1.42 \times 10^{-47}$) GO terms. The wheat module W05 is enriched for disease resistance
230 (TO:0000112, $p = 2.55 \times 10^{-178}$), suggesting that despite the continued symptomless
231 infection the host is already expressing genes for defence. Four genes in module F16 result
232 in reduced virulence when individually deleted. These are *FgNPC1* (sterol trafficking)
233 (Breakspear et al., 2011), *FgSrp2* (mRNA splicing) (Zhang et al., 2020), and the transcription
234 factors *Gzcon7* and *Gzc2h045* (Son et al., 2011) (**Table 1, Supplementary File 2**).
235 However, no gene deletion mutants exhibiting a loss of pathogenicity or highly reduced
236 virulence phenotype have yet been identified within this module, even though the eigengene
237 expression pattern clearly indicates an association with the early establishment of the fungus
238 in this key host tissue.
239 To identify genes in F16 that are likely involved in virulence, the 74 genes within this module
240 were examined. Key genes were defined as those exhibiting elevated module membership
241 (MM) within the module, which were also strongly correlated ($R > |0.70|$) with corresponding
242 wheat modules. Genes with a high MM value have expression patterns closely aligned with
243 the module's overall eigengene expression and are the most representative of the module.
244 The initial candidate gene list was selected by starting with the 15 key genes with the highest
245 MM within the module. Genes were then excluded that were likely to have functional
246 redundancy (i.e. belonged to a gene family or had ancient paralogues within PH-1) to avoid
247 compensatory effects when performing single gene deletion (**Supplementary Table S1**).

248 Ultimately, only two genes met these criteria: FGRAMPH1_0T23707 and
249 FGRAMPH1_01T27545. FGRAMPH1_01T27545 has been previously characterised as the
250 Niemann–Pick type C gene (*FgNPC1*). *FgNPC1* is necessary for sterol trafficking, with its
251 deletion resulting in ergosterol accumulation within the vacuole and a reduced virulence
252 upon wheat infection (Breakspear et al., 2011). Orthologue analysis identified that the
253 FGRAMPH1_0T23707 gene was a 1:1 orthologue of Killer-nine resistant 4 (KNR4) in
254 *Saccharomyces cerevisiae* (Martin et al., 1999), therefore the orthologue in *F. graminearum*
255 is henceforth referred to as *FgKnr4*.

256 ***FgKnr4*, a key gene of module F16, is necessary for**
257 **establishment of fungal infection**

258 *FgKnr4* was deleted using a split hygromycin replacement cassette (**Figure 6 – figure**
259 **supplement 1 A-B**). *T. aestivum* cv. Bobwhite was inoculated at anthesis with three
260 independent $\Delta Fgknr4$ transformants. No symptomatic disease progression past the
261 inoculated spikelets was observed with each $\Delta Fgknr4$ transformant (**Figure 5 A-B**). While
262 the inoculated spikelets developed symptoms, these did not exhibit full bleaching of the
263 spikelet characteristic of FHB infection. Instead, eye-shaped lesions formed akin to those
264 evident following $\Delta Fgtri5$ mutant infection (**Figure 5C**) (Cuzick et al., 2008). Plating of
265 surface sterilised wheat dissected into its constituent parts revealed the absence of fungal
266 growth in un-inoculated spikelets (**Figure 5 – figure supplement 1**). Nevertheless, browning
267 was noted in the rachis tissue immediately adjacent to the point inoculated spikelet,
268 accompanied by fungal growth. However, this colonisation did not occur past the rachis
269 internode of the 3rd spikelet. These data suggest that, despite entering the rachis, the
270 $\Delta Fgknr4$ mutant is unable to grow through the rachis node tissue and re-enter other
271 spikelets. Microscopic examination revealed a more pronounced plant defence response to
272 $\Delta Fgknr4$ infection. This was characterised by a visibly reduced fungal burden (**Figure 5D**).
273 Despite highly reduced virulence, DON mycotoxin was detected in the inoculated spikelet

274 and attached rachis internodes (≥ 0.2 ppm). However, DON was undetectable in the
275 neighbouring uninoculated spikelet (< 0.2 ppm). Complementation of the mutant with wild-
276 type *FgKnr4* restored virulence to wild-type levels (**Figure 5 E-F**).

277

278 ***FgKnr4* influences cell wall structure, stress resistance,
279 and growth**

280 *In vitro* growth of $\Delta Fgknr4$ was examined by culturing the fungus on both high or low nutrient
281 agar. In both conditions a decreased growth rate relative to the wild-type was apparent
282 (**Figure 6A, Figure 6 – figure supplement 1 and 2**). In addition to this, conidia of $\Delta Fgknr4$
283 appear smaller than wild-type (**Figure 6 – figure supplement 3 A,C**). Despite these
284 morphological differences $\Delta Fgknr4$ retains the ability to produce perithecia and ascospores,
285 albeit 8 days later than the wild-type (**Figure 6 – figure supplement 3 D-E**).

286 Stresses encountered by the fungus during *in planta* infection were mimicked *in vitro* using
287 chemical stressors. $\Delta Fgknr4$ had increased susceptibility to osmotic stress (1.5M NaCl),
288 oxidative stress (H_2O_2), and calcofluor white induced cell wall damage compared to the wild-
289 type and complemented strains (**Figure 6A, Figure 6 – figure supplement 1C & 2C**).

290 These susceptibilities may be due to changes in the cell wall structure of the $\Delta Fgknr4$ strain.
291 Corroborating this hypothesis, staining for chitin found an irregular deposition of chitin on the
292 $\Delta Fgknr4$ conidial cell wall, specifically along the tips and septa of the conidia (**Figure 6B,**
293 **Figure 6 – figure supplement 4**). Furthermore, an irregular cell wall structure was observed
294 upon transmission electron microscopy (TEM) analysis of the $\Delta Fgknr4$ conidia, indicative of
295 an abnormal cell wall composition (**Figure 6C, Figure 6 – figure supplement 5**).

296 The *FgKnr4* (F16) module was correlated with the wheat module W05, which exhibits a
297 significant enrichment in the term oxidative stress (TO: 0002657; $p = 3.88 \times 10^{-34}$) that
298 encompasses a total of 1143 genes. Among these genes are two respiratory burst oxidase

299 homologues (RBOH), specifically a predicted homolog of RBOF (TraesCS1A02G347700)
300 and RBOHE (TraesCS5D02G222100), along with predicted catalase homologues, CAT3
301 (TraesCS7B02G473400) (Ghorbel et al., 2023; Yan Zhang et al., 2022), and two CAT4
302 genes (TraesCS5B02G023300, TraesCS5D03G0079400) (Andleeb et al., 2022). W05 is
303 also enriched for sodium content (TO: 0000608; $p = 0.00014$) and salt tolerance (TO:
304 0006001; $p = 3.00 \times 10^{-18}$). The necessity of a functional *FgKnr4* gene in oxidative and
305 osmotic stress tolerance (**Figure 6A, Figure 6 – figure supplement 1C & 2C**) suggests that
306 *FgKnr4* is critical during this early infection stage, where the fungus confronts hydrogen
307 peroxide and osmotic stress induced by the plant.

308 The involvement of *FgKnr4* in cell wall metabolism was further studied by examining its
309 effect on the cell wall integrity pathway (CWI). The fungal CWI pathway is triggered in
310 response to various stresses (e.g. oxidative stress, osmotic pressure, cell wall damage)
311 (Dichtl et al., 2016) and in *F. graminearum* is activated through the phosphorylation of the
312 MAP-kinase (MAPK) *FgMGV1* (Hou et al., 2002; Yun et al., 2014). A Western blot was run
313 on mycelium samples grown with and without a cell wall stress (calcofluor white).
314 Constitutive activation of MGV1 in the absence of stress and increased phosphorylation
315 under stress was observed in $\Delta Fgknr4$ when compared to the wild-type (**Figure 6D-E**). This
316 finding is consistent with previous observations in *S. cerevisiae* (Martin-Yken et al., 2003).
317 This reinforces the biological function of *FgKnr4*, suggesting an involvement in fungal stress
318 responses and cell wall morphology in *F. graminearum*.

319 **The orthologous gene in wheat pathogen *Zymoseptoria*
320 *tritici* is also important for cell wall integrity and virulence
321 on wheat**

322 Analysis of the Knr4 protein conservation found that orthologues were highly distributed
323 across the Dikarya, occurring in both Ascomycota and Basidiomycota (**Figure 7**). Notably,

324 no orthologues of the gene were found in other Eukaryotes, highlighting its specificity to the
325 fungal lifestyle. This high level of conservation across fungi suggests that phenotypes
326 observed in *F. graminearum* may also be conserved in other economically significant
327 pathogenic fungi.

328 The orthologous *KNR4* gene in another wheat fungal pathogen *Z. tritici* (*ZtKnr4*,
329 Mycgr3G105330) was disrupted to test for conserved gene function. Despite the
330 phylogenetic distance between the two fungi, the *FgKnr4* and *ZtKnr4* proteins share 43.5%
331 pairwise identity. Mirroring the phenotype observed in *F. graminearum*, reduced virulence
332 (chlorosis but limited to no necrosis) was observed when wheat leaves were inoculated with
333 $\Delta ZtKnr4$ (**Figure 8A**). In addition to this the $\Delta ZtKnr4$ mutant was susceptible to calcofluor
334 white induced cell wall stress and exhibited reduced hyphal branching (**Figure 8B-C**). These
335 results highlight the potential of employing the *Fusarium*-wheat dual co-expression approach
336 to gain insights into fungal-plant interactions, both within *Fusarium* species and across the
337 fungal kingdom.

338

339 Discussion

340 The generated dual *F. graminearum*-wheat co-expression network was successfully used to
341 identify a gene necessary for virulence. By analysing stage-specific modules of infection,
342 module F16 was identified, which exhibited high gene expression levels during the
343 symptomless stage of FHB infection. Within this module, the gene *FgKnr4* was found to
344 have a high module membership score, indicating its central role in the module.
345 Experimental validation showed that *FgKnr4* is essential for responding to chemical
346 compounds that induce cell wall stress, early establishment of *in planta* infection, and
347 subsequent disease progression in wheat spikes. Similarly, the deletion of *Knr4* in another
348 pathogenic species, namely *Z. tritici* resulted in a reduced virulence phenotype in leaves and
349 displayed a comparable cell wall stress phenotype. This highlights the utility of pathogen-

350 host co-expression network analysis in identifying conserved virulence genes across wheat
351 fungal pathogens.

352 The predictions from the WGCNA were validated for the F12-W12 correlation through the
353 experimental confirmation of the co-regulation of the Fusarium trichothecene mycotoxin and
354 wheat detoxification genes during infection. For Fusarium, module F12 was of exceptionally
355 high interest because of its positioning specifically at the transition between the late
356 symptomless stage and the early symptomatic stage. For wheat genes in the correlated
357 module W12, the studied genes included two phenylalanine ammonia-lyases (*PAL* 1 and 2)
358 along with a predicted detoxifying efflux transporter (*TaDTX16*). Although *TaPAL* 1 and 2
359 have not been previously studied for their direct involvement in disease resistance in the
360 wheat - Fusarium interaction, the *PAL* gene family is known to be associated with disease
361 resistance and other phenotypes (Duba et al., 2019). In multiple plant species (including
362 *Arabidopsis*, pepper (*Capsicum annuum*), and rice (*Oryza sativa*)), *PAL* is induced in
363 response to biotic and abiotic stresses, which includes pathogen induced stress, (Hahlbrock
364 and Scheel, 1989; Kim and Hwang, 2014; Tonnessen et al., 2015; Chen et al., 2017) and in
365 numerous genetically incompatible host-pathogen interactions mediated by cognate R-Avr
366 proteins including responses to fungi (Maher et al., 1994; Ramaroson et al., 2022). *TaDTX16*
367 is part of the multidrug and toxic compound extrusion (MATE) gene family and was named
368 after its orthologue in *Arabidopsis thaliana* (Li et al., 2002). DTX/MATE take part in heavy
369 metal and lethal compound detoxification in plants and could be involved in mycotoxin
370 detoxification (Perincherry et al., 2019). Previously, a wheat DTX gene was reported to be
371 highly expressed in resistant cultivars of wheat compared to a susceptible wheat cultivar
372 when infected with *F. graminearum* (Pan et al., 2018). *TaDTX16* is located on chromosome
373 5BL within an interval harbouring a resistance QTL for defence against the necrotrophic
374 fungal disease Septoria nodorum blotch (Li et al., 2021).

375 The characterisation of *FgKnr4*, underscores the importance of identifying genes necessary
376 for full virulence through gene expression studies. This approach is essential because

377 predicting the pathogenic potential of *Fusarium* species based solely on comparative
378 genomics is challenging due to the absence of significant differences in secreted effector
379 proteins, carbohydrate-active enzymes, or gene repertoires between pathogenic and
380 endophytic strains of *Fusarium* and *Fusarioid* species (Hill et al., 2022). *FgKnr4* was
381 investigated further for its multifaceted roles in growth, stress response, and cell wall
382 integrity. Supporting previous findings in *Fusarium asiaticum* (Yu Zhang et al., 2022), this
383 study demonstrates that *FgKnr4* is involved in regulating growth rate, conidial spore
384 morphology, and sensitivity to osmotic and oxidative stresses, as well as virulence and cell
385 wall stress tolerance in *F. graminearum*. Moreover, this study establishes that KNR4
386 influences the well-studied cytoplasmically located Mgv1 cell wall integrity (CWI) MAPK
387 pathway (Xu et al., 2022), resulting in visible abnormalities of the conidial cell wall (**Figure**
388 **6C, Figure 6 – figure supplement 5**). The cell wall integrity pathway in *F. graminearum* is
389 well-characterised, with each MAP-kinase in the cascade having been identified, studied,
390 and shown to have roles in virulence and/or asexual and sexual spore formation (Hou et al.,
391 2002; Jenczmionka et al., 2003; Urban et al., 2003; Zheng et al., 2012). Through
392 experimental validation, our findings reveal an additional layer of control within the *F.*
393 *graminearum* cell wall integrity pathway mediated by *FgKnr4*. This discovery contributes to
394 and further improves our understanding of the regulatory mechanisms governing cell wall
395 integrity in *F. graminearum*. This new finding also, offers the first insights into the regulatory
396 effects of KNR4 in a filamentous fungus. This additional knowledge aid the development of
397 novel strategies to mitigate losses caused by FHB disease and DON contamination.

398 *Z. tritici* possesses one of the most expansive publicly available eukaryotic pangenomes,
399 with approximately 42% of its genes categorised as accessory (Plissonneau et al., 2018).
400 *ZtKnr4* is part of the core *Z. tritici* genome of the European pangenome (Chen et al., 2023)
401 and designated within the core orthogroup OG0008320 within the global (Europe, Asia,
402 North and South America, Australia and Africa) pangenome (Badet et al., 2020). Given the
403 highly variable nature of accessory chromosomes in *Z. tritici*, the assignment of *ZtKnr4* to the

404 core genome in two separate pangenomic analyses underscores its importance in fungal
405 physiology. *ZtKnr4* is also expressed throughout the wheat infection process (Rudd et al.,
406 2015). Disruption of the gene resulting in a reduced virulence phenotype reinforces the
407 potential of *ZtKnr4* as a candidate target for fungicide development, emphasising its
408 significance in combating *Z. tritici* infections and mitigating agricultural losses. Despite the
409 ever present global importance of STB disease for many decades (Dean et al., 2012; Savary
410 et al., 2019) *Z. tritici* has far fewer functionally characterised genes, with only 99 genes with
411 a characterised phenotype within the Pathogen Host-Interactions database and only 50 of
412 these genes associated with a loss in pathogenicity or reduced virulence (Urban et al., 2022;
413 Cuzick et al., 2023). The reduced virulence phenotype observed in the *ZtKnr4* mutant
414 therefore marks a valuable contribution to the characterisation of one of the >9000 core
415 genes across the known *Z. tritici* pangenomes (Badet et al., 2020; Chen et al., 2023).

416 The high conservation and exclusivity of KNR4 within the fungal kingdom, combined with its
417 absence in other eukaryotes and its conserved function across related species, suggest that
418 KNR4 could be an ideal target for intervention. This could be achieved through the
419 development of chemical fungicides that disrupt the protein's function (Aamir et al., 2018) or
420 through the application of RNA interference techniques (Cools and Hammond-Kosack, 2013;
421 Machado et al., 2018; Mann et al., 2023). Stricter EU regulation of chemicals suitable for
422 fungicide use in agricultural, medical and/or veterinary settings (European Commission,
423 2022), combined with significant losses in fungicide efficacy due to the evolution of pathogen
424 populations means there is a pressing need to identify new target sites for control.
425 Therefore, this research not only advances our understanding of fungal virulence
426 mechanisms but also offers promising directions for the development of effective strategies
427 for disease control in agriculture.

428 Materials and Methods

429 Gene co-expression network analysis

430 RNAseq reads from Dilks et al. (2019) were provided by Dr Neil Brown (European
431 Nucleotide Archive: PRJEB75530). Read quality was assessed with FastQC v. 0.11.9
432 (Andrews, 2010). Reads were mapped to a combined *Fusarium* – wheat genome, consisting
433 of v. 5 of the *Fusarium graminearum* PH-1 genome (King et al., 2017) and the high
434 confidence (HC) transcripts of the v. 2.1 of the International Wheat Genome Sequencing
435 Consortium (IWGSC) *Triticum aestivum* genome (Zhu et al., 2021). Genome indexing and
436 read alignment were performed using STAR aligner 2.7.8a. Soft clipping was turned off to
437 prevent reads incorrectly mapping to similar regions of the highly duplicated hexaploid wheat
438 genome. Reads were filtered using the filterByExpr function part of the R package Edge R
439 v.3.32.1 (Robinson et al., 2010). Counts were normalised separately for fungal and wheat
440 reads by performing a variance stabilising transformation (VST) using the DESeq2 v 1.30.1
441 R package (Love et al., 2014) in R (v4.0. 2, <https://www.r-project.org/>).

442 The VST normalised counts were filtered to remove any excessive missing values using the
443 function goodSamplesGenesMS in the WGCNA R package (Langfelder and Horvath, 2008).
444 Standard methods were implemented to generate the network using the WGCNA R
445 package, with the following parameters. A signed-hybrid network was constructed using the
446 filtered counts. The soft thresholding power (β) was uniquely selected per network according
447 to scale free model criteria (Zhang and Horvath, 2005), where $\beta = 9$ for the fungal network
448 and $\beta = 18$ for the wheat network (**Figure 2 – figure supplement 2**). A deepSplit of 3 was
449 paired with a standard cutheight of 0.25. A minimum module size of 50 was selected to
450 minimise potential transcriptional noise when assigning modules using smaller datasets
451 (Oldham, 2014; Walsh et al., 2016). The function multiSetMEs from the WGCNA package
452 was used to calculate module eigengene expression. Module eigengenes with similar
453 expression profiles were then merged.

454 Module quality and preservation was calculated using the function modulePreservation
455 present in the WGCNA R package (Langfelder and Horvath, 2008; Langfelder et al., 2011).
456 When calculating module preservation, the original wheat or fungal network was considered

457 the reference network. Then 50 different test networks were created, each built upon
458 randomly resampling (with replacement) a proportion of samples from the original dataset.
459 The average preservation metrics (i.e. Z-score) between the original network and the 50 test
460 networks was calculated for both the fungal and wheat networks.

461 **Module Enrichment an Annotation**

462 Gene ontology (GO) annotations of the v. 5 PH-1 genome (GCA_900044135.1) were
463 generated using Blast2GO v .5 (Götz et al., 2008). Enrichment was calculated using a
464 background set of all genes present in the fungal network. GO annotations for the IWGSC
465 v.2.1 genome were provided by Dr Keywan Hassani-Pak of the KnetMiner team (Hassani-
466 Pak et al., 2021). This was generated by performing a BLASTx search on the NCBI nb
467 database using DIAMOND v 2.0.13-GCC-11.2.0 (Buchfink et al., 2015), then Blast2GO v.5
468 was used to annotate the BLAST hits with GO terms. GO term enrichment was calculated for
469 each high level GO ontology (Biological Process, Molecular Function and Cellular
470 Component) using the R package topGO v 2.46.0 (Alexa and Rahnenfuhrer, 2009).

471 Plant Trait Ontology (TO) (Cooper et al., 2024) enrichment analysis was performed using
472 annotations derived from the KnetMiner knowledge graph (release 51) for wheat (Hassani-
473 Pak et al., 2021) and KnetMiner datasets and enrichment analysis notebooks are available
474 at <https://github.com/Rothamsted/knetgraphs-gene-traits/>. Predicted effectors were
475 determined using EffectorP v.3.0 (Sperschneider and Dodds, 2022). Alongside this,
476 predictions to identify extracellularly localised genes were done using SignalP v6.0 (Teufel et
477 al., 2022). Custom *F. graminearum* gene set enrichment of the network modules was
478 calculated by performing a Fisher's exact test using all the genes in the fungal network as
479 the background gene set. A BH correction was calculated for both GO and custom
480 enrichments (Benjamini and Hochberg, 1995). Modules were deemed significantly enriched
481 if P-corr < 0.05.

482 Gene lists included in GSEA consisted of predicted secreted effector proteins, alongside
483 known gene families associated with virulence, such as biological metabolite clusters
484 (BMCs) (Sieber et al., 2014), polyketide synthases (Gaffoor et al., 2005), protein kinases
485 (Wang et al., 2011) and transcription factors (Son et al., 2011). Due to their well-established
486 importance in *F. graminearum* pathology, a separate enrichment for genes of the *TRI* gene
487 cluster was also performed.

488 Annotation from PHI-base was obtained by mapping genes to version PHI-base (v4.16)
489 annotation using UniProt gene IDs and any through Decypher Tera-Blast™ P (TimeLogic,
490 Inc. Carlsbad, California, USA) (E-value = 0) against the PHI-base (v4.16) BLAST database
491 (Cuzick et al., 2023).

492 **Fungal material and growth conditions**

493 *F. graminearum* strains were cultured and conidia prepared as previously described (Brown
494 et al., 2010). Fungal strains were grown for 4 days on nutrient-rich potato dextrose agar
495 (PDA), nutrient-poor synthetic nutrient agar (SNA; 0.1% KH₂PO₄, 0.1% KNO₃, 0.1%
496 MgSO₄·7H₂O, 0.05% KCL, 0.02% glucose, 0.02% sucrose and 2% agar) and PDA with
497 different cell wall stresses. Plates were point inoculated with 20 µl of 4-fold dilution series
498 starting with 1 x 10⁶ conidia/ml. For the growth rate assay, fungi were grown on PDA and
499 images were taken at 7 days. Surface sterilisation of wheat spikes was performed by
500 submerging single wheat spikelets in 1/8 diluted thin bleach for 3 min, followed by three
501 washes with distilled H₂O. Dissection was done using a razor blade to separate the point
502 inoculated spikelets and adjacent spikelets (**Figure 5 – supplement 1**). Wheat tissue was
503 placed on SNA and images taken after 3-day incubation at room temperature in the dark.
504 Perithecia induction was achieved as described in Cavinder et al. (2019). All plate images
505 were taken using an Olympus OM-D camera using a 60mm ED M.Zuiko macro lens. Conidia
506 and ascospore images were taken using the Axiomager 2 (Zeiss, Oberkochen, Germany)

507 under brightfield illumination. Conidia lengths (N=50) and perithecia heights (N= 50) were
508 measured using ImageJ (Schneider et al., 2012).

509 ***Fusarium graminearum* genetic manipulations**

510 The *FgKnr4* gene was deleted through split marker-mediated transformation targeted fungal
511 replacement with the hygromycin by homologous recombination (Yu et al., 2004). *F.*
512 *graminearum* gene deletion construct assembly and fungal transformation was preformed
513 following methods outlined in King et al., 2017. Primers were designed for the fusion of the 5'
514 and 3' constructs using the NEBbuilder® Assembly Tool v.1 (<https://nebulerv1.neb.com/>).
515 Using the Gibson Master Mix (New England Biolabs, UK) the paired split marker fragments
516 were ligated into the pGEM® - T Easy Vector (Promega, UK) then transformed into DH5α
517 competent *Escherichia coli* (C2987H, New England Biolabs, UK) following standard
518 manufacturer protocol. Diagnostic PCRs done using DreamTaq polymerase
519 (ThermoFisher, UK) and standard cycling conditions. For the single gene deletion, three
520 separate transformants two diagnostic PCRs detect the presence of the replacement
521 cassette flanks (P3-4,P5-6) and the absence of the wild-type gene (P1-2) (**Figure 6 – figure**
522 **supplement 1 A-B**). Complementation was performed following the protocol developed by
523 Darino et al. (2024). Diagnostic PCRs for the complemented strains involved amplification of
524 insertion cassette flanks (P7-8; P9-10), absence of short 868 bp empty intragenic locus
525 amplicon (P11-P12), and test for heterozygosity of geneticin gene (P13-P14) (**Figure 6 –**
526 **figure supplement 2 A-B**. Full primer list available in Supplementary File 3.

527 **Wheat host inoculation**

528 The susceptible spring wheat (*T. aestivum*) cultivar, Bobwhite, was grown to anthesis. The
529 5th and 6th spikelets from the top of the wheat spike were inoculated on both sides using 5
530 μ l of 5×10^5 conidia/ml. Each treatment included 10 separate wheat plants (N=10). After
531 inoculation, plants were kept in a high humidity chamber for 48 h in the dark. Disease

532 progression was documented every two days by scoring the number of bleached spikelets.
533 At 15 dpi wheat spikelet tissue and adjacent rachis internode was separated, frozen in liquid
534 nitrogen, and ground to form a fine powder. The presence of DON mycotoxin was assessed
535 using the Deoxynivalenol (DON) Plate Kit (Cat. 20-0016, Beacon Analytical Systems Inc.,
536 USA) following standard protocol. Experiment was replicated with three biological replicates
537 per treatment (N=3). All plate images were taken using an Olympus OM-D camera using a
538 60mm ED M.Zuiko macro lens.

539

540 For resin dissection microscopy wheat cv. Bobwhite was inoculated 7th and 8th true spikelets
541 from base inoculated each side w/ 5x10⁵ spores /ml in dH₂O. After inoculation, plants were
542 kept in a high humidity chamber for 48 h in the dark. Lemma tissues were excised from
543 infected spikelets at 7 dpi, fixed in a 4% paraformaldehyde, 2.5% glutaraldehyde solution
544 with 0.05M Sorensen's phosphate buffer (NaH₂PO₄:Na₂HPO₄, pH 7.0). Samples then
545 underwent 3 further buffer washes, a subsequent ethanol dehydration protocol (0-100%
546 EtOH) over 48hrs and LR White resin (TAAB) infiltration diluted with dry ethanol at
547 increasing ratios (1:4, 2:3, 3:2, 4:1, 100%). Samples were inserted into capsules (TAAB) and
548 resin polymerised at 60°C for 16 hours in a nitrogen oven (TAAB). Ultra-thin 1µm sections of
549 samples were cut on an ultramicrotome (Reichert-Jung, Ultracut) with glass knives, placed
550 onto glass polysine slides (Sigma Aldrich, UK), dried at 70°C, stained with 0.1% (w/v)
551 Toluidine Blue O and mounted in DPX mounting medium (Fisher Scientific). Stained sections
552 were imaged on a Zeiss Axioimager (Axiocam 512 color, Zeiss, Jena, Germany) light
553 microscope with brightfield illumination.

554 **Gene expression of module W12 genes**

555 Bobwhite wheat plants were point inoculated at anthesis with either wild-type PH-1, $\Delta Fgr15$
556 or water only (Mock) following the protocol outlined in Dilks et al., (2019). Each experimental
557 condition was replicated in triplicate, with each replicate deriving from three pooled

558 independent wheat spikes. Tissues from rachis internodes 1 and 2 were sampled and frozen
559 in liquid nitrogen at 3 dpi. Frozen samples were ground and RNA was extracted using the
560 Monarch® Total RNA Miniprep Kit (NEB, UK). Equal amounts of RNA was used to
561 synthesise cDNA with Revertaid cDNA synthesis kit (ThermoScientific, UK). PowerTrack™
562 SYBR Green Master Mix (ThermoScientific, UK) was used for qPCR. Each biological
563 replicate included three technical replicates.

564 **Western blot**

565 A 200 ul aliquot of a *F. graminearum* spore solution (1×10^6 spores/ml) was added to 10 ml
566 potato dextrose broth (PDB) at 27 °C. Calcofluor white was added to a concentration of 200
567 µg/ml after 24 h of incubation at 180 rpm. Twenty-four hours after the addition of the stress,
568 mycelium was harvested, flash frozen and freeze dried To lyse the samples Y-PER Yeast
569 Protein Extraction Reagent (ThermoScientific, UK) was added to the freeze-dried samples at
570 1.5 ml per 150 mg tissue, alongside Protease Inhibitor Cocktail (100x) (ThermoScientific,
571 UK). Samples were lysed using the FastPrep-24™ machine for 20s (MP Biomedical, USA).
572 The supernatant was mixed with 5xSDS loading buffer (National Diagnostics, USA).

573 Equal amounts of protein (60 µg) were resolved on 8% SDS-PAGE gels (Mini-PROTEAN,
574 Bio-Rad, UK) and transferred on to a nitrocellulose membrane. Immunoblots were performed
575 by standard procedures using the Phospho-p44/42 MAPK (Erk1/2) (cat. #4370) and p44/42
576 MAPK (Erk1/2) (cat. #9102S) (Cell Signalling Technologies, USA) antibodies at their
577 specified dilutions. The blots were developed using ECL Plus Western Blotting Detection Kit
578 and images were acquired using Odyssey Imaging System (LI-COR Biosciences Ltd,
579 Cambridge, UK).

580 **Microscopic examination of cell wall**

581 Spores were induced by plating 200 µl of frozen spores (1×10^6) PDA and incubating plates
582 in for 3 days. For conventional transmission electron microscopy (TEM), fresh spores were

583 harvested the same day from the PDA plates and pellets were fixed in a mixture of 2.5%
584 glutaraldehyde and 4% Paraformaldehyde in Sorenson's buffer (SB) at pH 7.2 overnight at
585 4°C. The samples were rinsed in SB and post fixed in 1% osmium tetroxide for 60 min at
586 room temperature. The samples were dehydrated for 10 min per step into increasing
587 concentrations of alcohol (30%, 50%, 70%, 90% and final 100% \times 3). Subsequently, the pure
588 alcohol was replaced with propylene oxide, and the specimens were infiltrated with
589 increasing concentrations (25%, 50%, 75%, and 100%) of Spurr resin mixed with propylene
590 oxide for a minimum of 2 hr per step. The samples were embedded in pure, fresh Spurr resin
591 and polymerised at 60 °C for 24 hr. Ultrathin sections (70 nm) were cut using an
592 ultramicrotome (Leica UC7, Germany) and post-stained, first with uranyless for 1 min and
593 then with Reynolds lead citrate for 2 min at room temperature, prior to observation using a
594 Transmission Electron Microscope (Jeol 2100plus, UK) operated at 200 kV.

595 *F. graminearum* spore solution (1 x 10⁶ spores/ml) was stained with Wheat Germ Agglutinin,
596 Alexa Fluor™ 488 Conjugate (WGA) (10 μ g/ml) for 10 minutes each. Samples were washed
597 three times in sterile distilled water after staining. A ZEISS 780 Confocal Laser Scanning
598 Microscope (ZEISS, Germany) was used to image spores.

599 **Phylogenetic tree construction**

600 Eggnogmapper-v5 (Huerta-Cepas et al., 2019) was used to map *FgKnr4* to the eggno
601 Orthologue Group (OG) ENOG502QTAZ and generate the phylogenetic tree. The tree was
602 visualised and annotated using the interactive Tree of Life (iTOL) software (Letunic and
603 Bork, 2024).

604 **Functional characterisation of the *Knr4* orthologue in *Z. tritici***

605 ***tritici***

606 Separate analyses using Orthologous Matrix (OMA) (Altenhoff et al., 2021) and
607 Eggnogmapper (Huerta-Cepas et al., 2019) identified a single orthologous sequence in the

608 genome of *Z. tritici* isolate IPO323 (https://fungi.ensembl.org/Zymoseptoria_tritici/Info/Index)
609 (Goodwin et al., 2011). The gene has a Rothamsted gene model Id of
610 ZtritIPO323_04g12347 (King et al., 2017; Chen et al., 2023) and is present on Chromosome
611 8 at start position 230142 bp. This maps to Mycgr3P105330 in the current genome call on
612 Joint Genome Institute (JGI) Mycocosm (Goodwin et al., 2011).

613 Agrobacterium-mediated fungal transformation (Motteram et al., 2011) was performed to
614 generate a series of independent gene disruption mutants of *ZtKnr4*. Flanking sequences
615 and the hygromycin resistance gene were amplified from either genomic DNA or from
616 plasmid pCHYG and using Phusion polymerase (NEB, UK). Fragments were gel purified
617 using QIAquick Gel Extraction Kit (QIAGEN, UK) and assembled into the backbone (Kpn1
618 and BamH1 digested) of pCHYG by Gibson Assembly (NEB, UK). The resulting plasmids
619 were transformed into Agrobacterium strain AgL1 and fungal transformation of isolate
620 IPO323 was performed as per standard protocols (Motteram et al., 2011). Positive
621 transformants containing a disrupted *ZtKnr4* gene were identified by diagnostic PCR (**Figure**
622 **8 – figure supplement 1**). Complementation of validated *ZtKnr4* mutants was performed
623 through Agrobacterium-mediated transformation with plasmid pCGEN (digested EcoR1 and
624 Kpn1) containing the native gene plus 1 kb upstream (5') and 300 bp (3') downstream
625 genomic DNA, amplified by Phusion PCR (NEB, UK).

626 Attached leaf virulence assays were performed as per standard protocols (Keon et al., 2007)
627 on wheat cultivar Riband. Leaf blades (N = 3) were inoculated with spore suspensions of 1 x
628 10⁶ spores / ml in sterile water + 0.05% v:v Tween 20. Final disease assessments were
629 made 21 days after inoculation. *In vitro* hyphal growth assays were performed following
630 droplet inoculation of spore suspensions onto 1% Tap Water Agar (TWA) plates. Hyphal
631 growth morphologies were determined by light microscopy and / or photography 10 days
632 after inoculation. Calcofluor white sensitivity assays were performed to ascertain changes in
633 cell wall strength. For this, spore suspensions were inoculated onto YPD agar (Formedium,
634 UK) plates (control) and onto YPD agar plates containing 200 µg / ml calcofluor white. Plates

635 were incubated at RT for 8 days and then growth was monitored and recorded by
636 photography. Images of *ZtKnr4* in *planta* and *in vitro* experiments were taken with a Nikon
637 D3200 camera.

638 Data availability

639 Full lists of all genes clustered into modules is available on
640 https://github.com/erikakroll/Fusarium-wheat_WGCNA. This includes comma
641 separated value (CSV) files for all genes in each module for both fungal and wheat
642 modules, which are annotated with Module Membership (MM) values, mean FPKM
643 values, InterPro annotation, Gene Ontology annotation, and Trait Ontology
644 annotation. Text documents containing module eigengene values and gene module
645 assignments are also available on the repository.

646

647 References

648 Aamir M, Singh VK, Dubey MK, Meena M, Kashyap SP, Katari SK, Upadhyay RS,
649 Umamaheswari A, Singh S. 2018. In silico Prediction, Characterization,
650 Molecular Docking, and Dynamic Studies on Fungal SDRs as Novel Targets
651 for Searching Potential Fungicides Against Fusarium Wilt in Tomato. *Front
652 Pharmacol* **9**:1038. doi:10.3389/fphar.2018.01038

653 AHDB. 2023. Risk assessment for fusarium mycotoxins in wheat | AHDB.
654 <https://ahdb.org.uk/mycotoxins>

655 Alexa A, Rahnenfuhrer J. 2009. Gene set enrichment analysis with topGO.
656 *Bioconductor Improv* **27**:1–26.

657 Altenhoff AM, Train C-M, Gilbert KJ, Mediratta I, Mendes de Farias T, Moi D, Nevers
658 Y, Radoykova H-S, Rossier V, Warwick Vesztrocy A, Glover NM, Dessimoz
659 C. 2021. OMA orthology in 2021: website overhaul, conserved isoforms,
660 ancestral gene order and more. *Nucleic Acids Res* **49**:D373–D379.
661 doi:10.1093/nar/gkaa1007

662 Andleeb T, Knight E, Borrill P. 2022. Wheat NAM genes regulate the majority of early
663 monocarpic senescence transcriptional changes including nitrogen
664 remobilization genes. *G3 GenesGenomesGenetics* **13**.
665 doi:10.1093/g3journal/jkac275

666 Andrews S. 2010. FastQC: a quality control tool for high throughput sequence data.

667 Armer V, Kroll, Erika, Darino, Martin, Urban, Martin, Smith, Dan, Hammond-Kosack
668 K. 2024. Navigating the *Fusarium* species complex: Host-Range Plasticity and
669 Genome Variations. Re-submitted post peer review for special issue in *Fungal*
670 *Biology*.

671 Arunachalam C, Doohan FM. 2013. Trichothecene toxicity in eukaryotes: Cellular
672 and molecular mechanisms in plants and animals. *Toxicol Lett* **217**:149–158.
673 doi:10.1016/j.toxlet.2012.12.003

674 Badet T, Oggeneuss U, Abraham L, McDonald BA, Croll D. 2020. A 19-isolate
675 reference-quality global pangenome for the fungal wheat pathogen
676 *Zymoseptoria tritici*. *BMC Biol* **18**:12. doi:10.1186/s12915-020-0744-3

677 Bai G, Su Z, Cai J. 2018. Wheat resistance to *Fusarium* head blight. *Can J Plant*
678 *Pathol*.

679 Benjamini Y, Hochberg Y. 1995. Controlling the False Discovery Rate: A Practical
680 and Powerful Approach to Multiple Testing. *J R Stat Soc Ser B Methodol*
681 **57**:289–300. doi:10.1111/j.2517-6161.1995.tb02031.x

682 Breakspear A, Pasquali M, Broz K, Dong Y, Kistler HC. 2011. Npc1 is involved in
683 sterol trafficking in the filamentous fungus *Fusarium graminearum*. *Fungal*
684 *Genet Biol FG B* **48**:725–730. doi:10.1016/j.fgb.2011.03.001

685 Brown JKM, Chartrain L, Lasserre-Zuber P, Saintenac C. 2015. Genetics of
686 resistance to *Zymoseptoria tritici* and applications to wheat breeding. *Fungal*
687 *Genet Biol* **79**:33–41. doi:10.1016/j.fgb.2015.04.017

688 Brown NA, Bass C, Baldwin TK, Chen H, Massot F, Carion PWC, Urban M, van de
689 Meene AML, Hammond-Kosack KE. 2011. Characterisation of the *Fusarium*
690 *graminearum*-Wheat Floral Interaction. *J Pathog* **2011**:e626345.
691 doi:10.4061/2011/626345

692 Brown NA, Evans J, Mead A, Hammond-Kosack KE. 2017. A spatial temporal
693 analysis of the *Fusarium graminearum* transcriptome during symptomless and
694 symptomatic wheat infection. *Mol Plant Pathol* **18**:1295–1312.
695 doi:10.1111/mpp.12564

696 Brown NA, Urban M, van de Meene AML, Hammond-Kosack KE. 2010. The infection
697 biology of *Fusarium graminearum*: defining the pathways of spikelet to
698 spikelet colonisation in wheat ears. *Fungal Biol* **114**:555–571.
699 doi:10.1016/j.funbio.2010.04.006

700 Buchfink B, Xie C, Huson DH. 2015. Fast and sensitive protein alignment using
701 DIAMOND. *Nat Methods* **12**:59–60. doi:10.1038/nmeth.3176

702 Buerstmayr M, Steiner B, Buerstmayr H. 2020. Breeding for *Fusarium* head blight
703 resistance in wheat—Progress and challenges. *Plant Breed* **139**:429–454.
704 doi:10.1111/pbr.12797

705 Cai H, Yu N, Liu Y, Wei X, Guo C. 2022. Meta-analysis of fungal plant pathogen
706 *Fusarium oxysporum* infection-related gene profiles using transcriptome
707 datasets. *Front Microbiol* **13**:970477. doi:10.3389/fmicb.2022.970477

708 Cavinder B, Sikhakolli U, Fellows KM, Trail F. 2012. Sexual Development and
709 Ascospore Discharge in *Fusarium graminearum*. *J Vis Exp* 3895.
710 doi:10.3791/3895

711 Chen H, King R, Smith D, Bayon C, Ashfield T, Torriani S, Kanyuka K, Hammond-
712 Kosack K, Bieri S, Rudd J. 2023. Combined pangenomics and transcriptomics
713 reveals core and redundant virulence processes in a rapidly evolving fungal
714 plant pathogen. *BMC Biol* **21**:24. doi:10.1186/s12915-023-01520-6

715 Chen Y, Li F, Tian L, Huang M, Deng R, Li X, Chen W, Wu P, Li M, Jiang H, Wu G.
716 2017. The Phenylalanine Ammonia Lyase Gene LjPAL1 Is Involved in Plant

717 Defense Responses to Pathogens and Plays Diverse Roles in *Lotus*
718 *japonicus*-Rhizobium Symbioses. *Mol Plant Microbe Interact* **30**:739–753.
719 doi:10.1094/MPMI-04-17-0080-R

720 Cools HJ, Hammond-Kosack KE. 2013. Exploitation of genomics in fungicide
721 research: current status and future perspectives. *Mol Plant Pathol* **14**:197–
722 210. doi:10.1111/mpp.12001

723 Cooper L, Elser J, Laporte M-A, Arnaud E, Jaiswal P. 2024. Planteome 2024
724 Update: Reference Ontologies and Knowledgebase for Plant Biology. *Nucleic*
725 *Acids Res* **52**:D1548–D1555. doi:10.1093/nar/gkad1028

726 Cuzick A, Seager J, Wood V, Urban M, Rutherford K, Hammond-Kosack KE. 2023.
727 A framework for community curation of interspecies interactions literature.
728 *eLife* **12**:e84658. doi:10.7554/eLife.84658

729 Cuzick A, Urban M, Hammond-Kosack K. 2008. *Fusarium graminearum* gene
730 deletion mutants map1 and tri5 reveal similarities and differences in the
731 pathogenicity requirements to cause disease on *Arabidopsis* and wheat floral
732 tissue. *New Phytol* **177**:990–1000. doi:10.1111/j.1469-8137.2007.02333.x

733 Darino M, Urban M, Kaur N, Machado Wood A, Grimwade-Mann M, Smith D,
734 Beacham A, Hammond-Kosack K. 2024. Identification and functional
735 characterisation of a locus for target site integration in *Fusarium*
736 *graminearum*. *Fungal Biol Biotechnol* **11**:2. doi:10.1186/s40694-024-00171-8

737 de Chaves MA, Reginatto P, da Costa BS, de Paschoal RI, Teixeira ML, Fuentefria
738 AM. 2022. Fungicide Resistance in *Fusarium graminearum* Species Complex.
739 *Curr Microbiol* **79**:62. doi:10.1007/s00284-021-02759-4

740 Dean R, Van Kan JAL, Pretorius ZA, Hammond-Kosack KE, Di Pietro A, Spanu PD,
741 Rudd JJ, Dickman M, Kahmann R, Ellis J, Foster GD. 2012. The Top 10
742 fungal pathogens in molecular plant pathology. *Mol Plant Pathol* **13**:414–430.
743 doi:10.1111/j.1364-3703.2011.00783.x

744 Desmond OJ, Manners JM, Stephens AE, Maclean DJ, Schenk PM, Gardiner DM,
745 Munn AL, Kazan K. 2008. The *Fusarium* mycotoxin deoxynivalenol elicits
746 hydrogen peroxide production, programmed cell death and defence
747 responses in wheat. *Mol Plant Pathol* **9**:435–445. doi:10.1111/j.1364-
748 3703.2008.00475.x

749 Dichtl K, Samantaray S, Wagener J. 2016. Cell wall integrity signalling in human
750 pathogenic fungi. *Cell Microbiol* **18**:1228–1238. doi:10.1111/cmi.12612

751 Dilks T, Halsey K, De Vos RP, Hammond-Kosack KE, Brown NA. 2019. Non-
752 canonical fungal G-protein coupled receptors promote *Fusarium* head blight
753 on wheat. *PLoS Pathog* **15**:e1007666. doi:10.1371/journal.ppat.1007666

754 Duba A, Goriewa-Duba K, Wachowska U, Głowacka K, Wiwart M. 2019. The
755 Associations between Leaf Morphology, Phenylalanine Ammonia Lyase
756 Activity, Reactive Oxygen Species, and *Fusarium* Resistance in Selected
757 Species of Wheat with Different Ploidy Levels. *Plants* **8**:360.
758 doi:10.3390/plants8100360

759 Dyer RB, Plattner RD, Kendra DF, Brown DW. 2005. *Fusarium graminearum* TRI14
760 is required for high virulence and DON production on wheat but not for DON
761 synthesis in vitro. *J Agric Food Chem* **53**:9281–9287. doi:10.1021/jf051441a

762 EFSA. 2017. Risks to human and animal health related to the presence of
763 deoxynivalenol and its acetylated and modified forms in food and feed |
764 EFSA. <https://www.efsa.europa.eu/en/efsajournal/pub/4718>

765 Estep LK, Torriani SFF, Zala M, Anderson NP, Flowers MD, McDonald BA, Mundt
766 CC, Brunner PC. 2015. Emergence and early evolution of fungicide resistance

767 in North American populations of *Zymoseptoria tritici*. *Plant Pathol* **64**:961–
768 971. doi:10.1111/ppa.12314

769 European Commission. 2022. Farm to Fork.
https://ec.europa.eu/commission/presscorner/detail/en/qanda_22_3694

770 European Commission. 2006. On the presence of deoxynivalenol, zearalenone,
771 ochratoxin A, T-2 and HT-2 and fumonisins in products intended for animal
772 feeding. *Off J Eur Union*, L 229/7.

773 Fones H, Gurr S. 2015. The impact of *Septoria tritici* Blotch disease on wheat: An EU
774 perspective. *Fungal Genet Biol* **79**:3–7. doi:10.1016/j.fgb.2015.04.004

775 Gaffoor I, Brown DW, Plattner R, Proctor RH, Qi W, Trail F. 2005. Functional
776 analysis of the polyketide synthase genes in the filamentous fungus
777 *Gibberella zeae* (anamorph *Fusarium graminearum*). *Eukaryot Cell* **4**:1926–
778 1933. doi:10.1128/EC.4.11.1926-1933.2005

779 Ghorbel M, Zribi I, Besbes M, Bouali N, Brini F. 2023. Catalase Gene Family in
780 Durum Wheat: Genome-Wide Analysis and Expression Profiling in Response
781 to Multiple Abiotic Stress Conditions. *Plants* **12**:2720.
782 doi:10.3390/plants12142720

783 Goodwin SB, M'barek SB, Dhillon B, Wittenberg AHJ, Crane CF, Hane JK, Foster
784 AJ, Van der Lee TAJ, Grimwood J, Aerts A, Antoniw J, Bailey A, Bluhm B,
785 Bowler J, Bristow J, van der Burgt A, Canto-Canché B, Churchill ACL, Conde-
786 Ferràez L, Cools HJ, Coutinho PM, Csukai M, Dehal P, De Wit P, Donzelli B,
787 van de Geest HC, van Ham RCHJ, Hammond-Kosack KE, Henrissat B, Kilian
788 A, Kobayashi AK, Koopmann E, Kourmpetis Y, Kuzniar A, Lindquist E,
789 Lombard V, Maliepaard C, Martins N, Mehrabi R, Nap JPH, Ponomarenko A,
790 Rudd JJ, Salamov A, Schmutz J, Schouten HJ, Shapiro H, Stergiopoulos I,
791 Torriani SFF, Tu H, de Vries RP, Waalwijk C, Ware SB, Wiebenga A, Zwijs
792 L-H, Oliver RP, Grigoriev IV, Kema GHJ. 2011. Finished genome of the fungal
793 wheat pathogen *Mycosphaerella graminicola* reveals dispensome structure,
794 chromosome plasticity, and stealth pathogenesis. *PLoS Genet* **7**:e1002070.
795 doi:10.1371/journal.pgen.1002070

796 Götz S, García-Gómez JM, Terol J, Williams TD, Nagaraj SH, Nueda MJ, Robles M,
797 Talón M, Dopazo J, Conesa A. 2008. High-throughput functional annotation
798 and data mining with the Blast2GO suite. *Nucleic Acids Res* **36**:3420–3435.
799 doi:10.1093/nar/gkn176

800 Hahlbrock K, Scheel D. 1989. Physiology and Molecular Biology of Phenylpropanoid
801 Metabolism. *Annu Rev Plant Physiol Plant Mol Biol* **40**:347–369.
802 doi:10.1146/annurev.pp.40.060189.002023

803 Hassani-Pak K, Singh A, Brandizi M, Hearnshaw J, Parsons JD, Amberkar S,
804 Phillips AL, Doonan JH, Rawlings C. 2021. KnetMiner: a comprehensive
805 approach for supporting evidence-based gene discovery and complex trait
806 analysis across species. *Plant Biotechnol J* **19**:1670–1678.
807 doi:10.1111/pbi.13583

808 Hill R, Buggs RJA, Vu DT, Gaya E. 2022. Lifestyle Transitions in Fusarioid Fungi are
809 Frequent and Lack Clear Genomic Signatures. *Mol Biol Evol* **39**.
810 doi:10.1093/molbev/msac085

811 Hou Z, Xue C, Peng Y, Katan T, Kistler HC, Xu J-R. 2002. A mitogen-activated
812 protein kinase gene (MGV1) in *Fusarium graminearum* is required for female
813 fertility, heterokaryon formation, and plant infection. *Mol Plant-Microbe
814 Interact MPMI* **15**:1119–1127. doi:10.1094/MPMI.2002.15.11.1119

815

816 Huerta-Cepas J, Szklarczyk D, Heller D, Hernández-Plaza A, Forslund SK, Cook H,
817 Mende DR, Letunic I, Rattei T, Jensen LJ, von Mering C, Bork P. 2019.
818 eggNOG 5.0: a hierarchical, functionally and phylogenetically annotated
819 orthology resource based on 5090 organisms and 2502 viruses. *Nucleic Acids*
820 *Res* **47**:D309–D314. doi:10.1093/nar/gky1085

821 Jansen C, von Wettstein D, Schäfer W, Kogel K-H, Felk A, Maier FJ. 2005. Infection
822 patterns in barley and wheat spikes inoculated with wild-type and trichodiene
823 synthase gene disrupted *Fusarium graminearum*. *Proc Natl Acad Sci*
824 **102**:16892–16897. doi:10.1073/pnas.0508467102

825 Jeger M, Beresford R, Bock C, Brown N, Fox A, Newton A, Vicent A, Xu X, Yuen J.
826 2021. Global challenges facing plant pathology: multidisciplinary approaches
827 to meet the food security and environmental challenges in the mid-twenty-first
828 century. *CABI Agric Biosci* **2**:20. doi:10.1186/s43170-021-00042-x

829 Jenczmionka NJ, Maier FJ, Lösch AP, Schäfer W. 2003. Mating, conidiation and
830 pathogenicity of *Fusarium graminearum*, the main causal agent of the head-
831 blight disease of wheat, are regulated by the MAP kinase gpmk1. *Curr Genet*
832 **43**:87–95. doi:10.1007/s00294-003-0379-2

833 John E, Singh KB, Oliver RP, Tan K-C. 2021. Transcription factor control of virulence
834 in phytopathogenic fungi. *Mol Plant Pathol* **22**:858–881.
835 doi:10.1111/mpp.13056

836 Johns LE, Bebber DP, Gurr SJ, Brown NA. 2022. Emerging health threat and cost of
837 *Fusarium* mycotoxins in European wheat. *Nat Food* **3**:1014–1019.
838 doi:10.1038/s43016-022-00655-z

839 Kanja C, Wood AKM, Baggaley L, Walker C, Hammond-Kosack KE. 2021. Cereal-
840 *Fusarium* interactions: Improved fundamental insights into *Fusarium*
841 pathogenomics and cereal host resistance reveals new ways to achieve
842 durable disease control. Achieving Durable Disease Resistance in Cereals.
843 Burleigh Dodds Science Publishing.

844 Kema GHJ, Yu D, Frits H. J R, Michael W. S, Robert P. B. 1996. Histology of the
845 Pathogenesis of *Mycosphaerella graminicola* in Wheat. *Phytopathology*
846 **86**:777–786.

847 Keon J, Antoniw J, Carzaniga R, Deller S, Ward JL, Baker JM, Beale MH,
848 Hammond-Kosack K, Rudd JJ. 2007. Transcriptional adaptation of
849 *Mycosphaerella graminicola* to programmed cell death (PCD) of its
850 susceptible wheat host. *Mol Plant-Microbe Interact MPMI* **20**:178–193.
851 doi:10.1094/MPMI-20-2-0178

852 Kim DS, Hwang BK. 2014. An important role of the pepper phenylalanine ammonia-
853 lyase gene (PAL1) in salicylic acid-dependent signalling of the defence
854 response to microbial pathogens. *J Exp Bot* **65**:2295–2306.
855 doi:10.1093/jxb/eru109

856 Kimura M, Tokai T, Takahashi-Ando N, Ohsato S, Fujimura M. 2007. Molecular and
857 genetic studies of fusarium trichothecene biosynthesis: pathways, genes, and
858 evolution. *Biosci Biotechnol Biochem* **71**:2105–2123. doi:10.1271/bbb.70183

859 King R, Urban M, Hammond-Kosack KE. 2017. Annotation of *Fusarium*
860 *graminearum* (PH-1) Version 5.0. *Genome Announc* **5**:e01479-16.
861 doi:10.1128/genomeA.01479-16

862 Kugler KG, Siegwart G, Nussbaumer T, Ametz C, Spannagl M, Steiner B, Lemmens
863 M, Mayer KF, Buerstmayr H, Schweiger W. 2013. Quantitative trait loci-
864 dependent analysis of a gene co-expression network associated with

915 Mateus ID, Masclaux FG, Aletti C, Rojas EC, Savary R, Dupuis C, Sanders IR. 2019.
916 Dual RNA-seq reveals large-scale non-conserved genotype \times genotype-
917 specific genetic reprogramming and molecular crosstalk in the mycorrhizal
918 symbiosis. *ISME J* **13**:1226–1238. doi:10.1038/s41396-018-0342-3

919 McDonald MC, Renkin M, Spackman M, Orchard B, Croll D, Solomon PS, Milgate A.
920 2019. Rapid Parallel Evolution of Azole Fungicide Resistance in Australian
921 Populations of the Wheat Pathogen *Zymoseptoria tritici*. *Appl Environ
922 Microbiol* **85**:e01908-18. doi:10.1128/AEM.01908-18

923 Motteram J, Lovegrove A, Pirie E, Marsh J, Devonshire J, van de Meene A,
924 Hammond-Kosack K, Rudd JJ. 2011. Aberrant protein N-glycosylation
925 impacts upon infection-related growth transitions of the haploid plant-
926 pathogenic fungus *Mycosphaerella graminicola*. *Mol Microbiol* **81**:415–433.
927 doi:10.1111/j.1365-2958.2011.07701.x

928 Nelson R. 2020. International Plant Pathology: Past and Future Contributions to
929 Global Food Security. *Phytopathology* **110**:245–253. doi:10.1094/PHYTO-08-
930 19-0300-IA

931 Nguyen T, Kröger C, Bönnighausen J, Schäfer W, Bormann J. 2013. The ATF/CREB
932 Transcription Factor Atf1 Is Essential for Full Virulence, Deoxynivalenol
933 Production, and Stress Tolerance in the Cereal Pathogen *Fusarium
934 graminearum*. *Mol Plant-Microbe Interact MPMI* **26**. doi:10.1094/MPMI-04-13-
935 0125-R

936 O'Donnell K, Kistler HC, Tacke BK, Casper HH. 2000. Gene genealogies reveal
937 global phylogeographic structure and reproductive isolation among lineages of
938 *Fusarium graminearum*, the fungus causing wheat scab. *Proc Natl Acad Sci
939* **97**:7905–7910. doi:10.1073/pnas.130193297

940 Oldham M. 2014. M. Transcriptomics: from differential expression to coexpression.
941 The OMICs: Applications in Neuroscience. Oxford University Press, UK.

942 Pan Y, Liu Z, Rocheleau H, Fauteux F, Wang Y, McCartney C, Ouellet T. 2018.
943 Transcriptome dynamics associated with resistance and susceptibility against
944 fusarium head blight in four wheat genotypes. *BMC Genomics* **19**:642.
945 doi:10.1186/s12864-018-5012-3

946 Park J, Lee H-H, Moon H, Lee N, Kim S, Kim J-E, Lee Y, Min K, Kim H, Choi GJ,
947 Lee Y-W, Seo Y-S, Son H. 2023. A combined transcriptomic and physiological
948 approach to understanding the adaptive mechanisms to cope with oxidative
949 stress in *Fusarium graminearum*. *Microbiol Spectr* **11**:e01485-23.
950 doi:10.1128/spectrum.01485-23

951 Perincherry L, Lalak-Kańczugowska J, Stępień Ł. 2019. Fusarium-Produced
952 Mycotoxins in Plant-Pathogen Interactions. *Toxins* **11**:664.
953 doi:10.3390/toxins11110664

954 Plissonneau C, Hartmann FE, Croll D. 2018. Pangenome analyses of the wheat
955 pathogen *Zymoseptoria tritici* reveal the structural basis of a highly plastic
956 eukaryotic genome. *BMC Biol* **16**:5. doi:10.1186/s12915-017-0457-4

957 Ramaroson M-L, Koutouan C, Helesbeux J-J, Le Clerc V, Hamama L, Geoffriau E,
958 Briard M. 2022. Role of Phenylpropanoids and Flavonoids in Plant Resistance
959 to Pests and Diseases. *Molecules* **27**:8371. doi:10.3390/molecules27238371

960 Robinson MD, McCarthy DJ, Smyth GK. 2010. edgeR: a Bioconductor package for
961 differential expression analysis of digital gene expression data. *Bioinforma
962 Oxf Engl* **26**:139–140. doi:10.1093/bioinformatics/btp616

963 Rudd JJ, Kanyuka K, Hassani-Pak K, Derbyshire M, Andongabo A, Devonshire J,
964 Lysenko A, Saqi M, Desai NM, Powers SJ, Hooper J, Ambroso L, Bharti A,

965 Farmer A, Hammond-Kosack KE, Dietrich RA, Courbot M. 2015.
966 Transcriptome and Metabolite Profiling of the Infection Cycle of *Zymoseptoria*
967 *tritici* on Wheat Reveals a Biphasic Interaction with Plant Immunity Involving
968 Differential Pathogen Chromosomal Contributions and a Variation on the
969 Hemibiotrophic Lifestyle Definition. *Plant Physiol* **167**:1158–1185.
970 doi:10.1104/pp.114.255927

971 Saldivar SOS. 2016. Cereals: Dietary Importance In: Caballero B, Finglas PM,
972 Toldrá F, editors. Encyclopedia of Food and Health. Oxford: Academic Press.
973 pp. 703–711. doi:10.1016/B978-0-12-384947-2.00130-6

974 Savary S, Willocquet L, Pethybridge SJ, Esker P, McRoberts N, Nelson A. 2019. The
975 global burden of pathogens and pests on major food crops. *Nat Ecol Evol*
976 **3**:430–439. doi:10.1038/s41559-018-0793-y

977 Schneider CA, Rasband WS, Eliceiri KW. 2012. NIH Image to ImageJ: 25 years of
978 image analysis. *Nat Methods* **9**:671–675. doi:10.1038/nmeth.2089

979 Sertsuvalkul N, DeMell A, Dinesh-Kumar SP. 2022. The complex roles of autophagy
980 in plant immunity. *FEBS Lett* **596**:2163–2171. doi:10.1002/1873-3468.14356

981 Shewry PR, Hey SJ. 2015. The contribution of wheat to human diet and health. *Food*
982 *Energy Secur* **4**:178–202. doi:10.1002/fes3.64

983 Shin Y-K, Kim D-W, Lee S-W, Lee M-J, Gi Baek S, Lee T, Yun S-H. 2022. Functional
984 roles of all five putative hydrophobin genes in growth, development, and
985 secondary metabolism in *Fusarium graminearum*. *Fungal Genet Biol*
986 **160**:103683. doi:10.1016/j.fgb.2022.103683

987 Sieber CMK, Lee W, Wong P, Münsterkötter M, Mewes H-W, Schmeitzl C, Varga E,
988 Berthiller F, Adam G, Güldener U. 2014. The *Fusarium graminearum* Genome
989 Reveals More Secondary Metabolite Gene Clusters and Hints of Horizontal
990 Gene Transfer. *PLOS ONE* **9**:e110311. doi:10.1371/journal.pone.0110311

991 Son H, Seo Y-S, Min K, Park AR, Lee J, Jin J-M, Lin Y, Cao P, Hong S-Y, Kim E-K,
992 Lee S-H, Cho A, Lee S, Kim M-G, Kim Y, Kim J-E, Kim J-C, Choi GJ, Yun S-
993 H, Lim JY, Kim M, Lee Y-H, Choi Y-D, Lee Y-W. 2011. A Phenome-Based
994 Functional Analysis of Transcription Factors in the Cereal Head Blight
995 Fungus, *Fusarium graminearum*. *PLoS Pathog* **7**:e1002310.
996 doi:10.1371/journal.ppat.1002310

997 Sperschneider J, Dodds PN. 2022. EffectorP 3.0: Prediction of Apoplastic and
998 Cytoplasmic Effectors in Fungi and Oomycetes. *Mol Plant-Microbe Interact*
999 *MPMI* **35**:146–156. doi:10.1094/MPMI-08-21-0201-R

1000 Steinberg G. 2015. Cell biology of *Zymoseptoria tritici*: Pathogen cell organization
1001 and wheat infection. *Fungal Genet Biol* **79**:17–23.
1002 doi:10.1016/j.fgb.2015.04.002

1003 Teufel F, Almagro Armenteros JJ, Johansen AR, Gíslason MH, Pihl SI, Tsirigos KD,
1004 Winther O, Brunak S, von Heijne G, Nielsen H. 2022. SignalP 6.0 predicts all
1005 five types of signal peptides using protein language models. *Nat Biotechnol*
1006 **40**:1023–1025. doi:10.1038/s41587-021-01156-3

1007 Tonnessen BW, Manosalva P, Lang JM, Baraoidan M, Bordeos A, Mauleon R, Oard
1008 J, Hulbert S, Leung H, Leach JE. 2015. Rice phenylalanine ammonia-lyase
1009 gene OsPAL4 is associated with broad spectrum disease resistance. *Plant*
1010 *Mol Biol* **87**:273–286. doi:10.1007/s11103-014-0275-9

1011 Torriani SFF, Melichar JPE, Mills C, Pain N, Sierotzki H, Courbot M. 2015.
1012 *Zymoseptoria tritici*: A major threat to wheat production, integrated
1013 approaches to control. *Fungal Genet Biol* **79**:8–12.
1014 doi:10.1016/j.fgb.2015.04.010

1015 Urban M, Cuzick A, Seager J, Wood V, Rutherford K, Venkatesh SY, Sahu J, Iyer
1016 SV, Khamari L, De Silva N, Martinez MC, Pedro H, Yates AD, Hammond-
1017 Kosack KE. 2022. PHI-base in 2022: a multi-species phenotype database for
1018 Pathogen–Host Interactions. *Nucleic Acids Res* **50**:D837–D847.
1019 doi:10.1093/nar/gkab1037

1020 Urban M, Mott E, Farley T, Hammond-Kosack K. 2003. The *Fusarium graminearum*
1021 MAP1 gene is essential for pathogenicity and development of perithecia. *Mol
1022 Plant Pathol* **4**:347–359. doi:10.1046/j.1364-3703.2003.00183.x

1023 Vicente I, Quaratiello G, Baroncelli R, Vannacci G, Sarrocco S. 2022. Insights on
1024 KP4 Killer Toxin-like Proteins of Fusarium Species in Interspecific
1025 Interactions. *J Fungi* **8**:968. doi:10.3390/jof8090968

1026 Walsh CJ, Batt J, Herridge MS, Mathur S, Bader GD, Hu P, dos Santos CC. 2016.
1027 Transcriptomic analysis reveals abnormal muscle repair and remodeling in
1028 survivors of critical illness with sustained weakness. *Sci Rep* **6**:29334.
1029 doi:10.1038/srep29334

1030 Wang C, Zhang S, Hou R, Zhao Z, Zheng Q, Xu Q, Zheng D, Wang G, Liu H, Gao X,
1031 Ma J-W, Kistler HC, Kang Z, Xu J-R. 2011. Functional analysis of the kinome
1032 of the wheat scab fungus *Fusarium graminearum*. *PLoS Pathog* **7**:e1002460.
1033 doi:10.1371/journal.ppat.1002460

1034 Xu M, Wang Q, Wang G, Zhang X, Liu H, Jiang C. 2022. Combatting Fusarium head
1035 blight: advances in molecular interactions between *Fusarium graminearum*
1036 and wheat. *Phytopathol Res* **4**:37. doi:10.1186/s42483-022-00142-0

1037 Yan X, Tang B, Ryder LS, MacLean D, Were VM, Eseola AB, Cruz-Mireles N, Ma W,
1038 Foster AJ, Osés-Ruiz M, Talbot NJ. 2023. The transcriptional landscape of
1039 plant infection by the rice blast fungus *Magnaporthe oryzae* reveals distinct
1040 families of temporally co-regulated and structurally conserved effectors. *Plant
1041 Cell* **35**:1360–1385. doi:10.1093/plcell/koad036

1042 Yu J-H, Hamari Z, Han K-H, Seo J-A, Reyes-Domínguez Y, Scazzocchio C. 2004.
1043 Double-joint PCR: a PCR-based molecular tool for gene manipulations in
1044 filamentous fungi. *Fungal Genet Biol FG B* **41**:973–981.
1045 doi:10.1016/j.fgb.2004.08.001

1046 Yun Y, Liu Z, Zhang J, Shim W-B, Chen Y, Ma Z. 2014. The MAPKK FgMkk1 of
1047 *Fusarium graminearum* regulates vegetative differentiation, multiple stress
1048 response, and virulence via the cell wall integrity and high-osmolarity glycerol
1049 signaling pathways. *Environ Microbiol* **16**:2023–2037. doi:10.1111/1462-
1050 2920.12334

1051 Zhang B, Horvath S. 2005. A general framework for weighted gene co-expression
1052 network analysis. *Stat Appl Genet Mol Biol* **4**:Article17. doi:10.2202/1544-
1053 6115.1128

1054 Zhang L, Zhou X, Li P, Wang Y, Hu Q, Shang Y, Chen Y, Zhu X, Feng H, Zhang C.
1055 2022. Transcriptome Profile of *Fusarium graminearum* Treated by Putrescine.
1056 *J Fungi* **9**:60. doi:10.3390/jof9010060

1057 Zhang Yu, Chen W, Shao W, Tan S, Shi D, Ma H, Chen C. 2022. FaSmi1 Is
1058 Essential for the Vegetative Development, Asexual Reproduction, DON
1059 Production and Virulence of *Fusarium asiaticum*. *J Fungi* **8**:1189.
1060 doi:10.3390/jof8111189

1061 Zhang Y, Dai Y, Huang Y, Wang K, Lu P, Xu H, Xu J-R, Liu H. 2020. The SR-protein
1062 FgSrp2 regulates vegetative growth, sexual reproduction and pre-mRNA
1063 processing by interacting with FgSrp1 in *Fusarium graminearum*. *Curr Genet*
1064 **66**:607–619. doi:10.1007/s00294-020-01054-2

1065 Zhang Yan, Zheng L, Yun L, Ji L, Li G, Ji M, Shi Y, Zheng X. 2022. Catalase (CAT)
1066 Gene Family in Wheat (*Triticum aestivum L.*): Evolution, Expression Pattern
1067 and Function Analysis. *Int J Mol Sci* **23**:542. doi:10.3390/ijms23010542
1068 Zheng D, Zhang S, Zhou X, Wang C, Xiang P, Zheng Q, Xu J-R. 2012. The FgHOG1
1069 Pathway Regulates Hyphal Growth, Stress Responses, and Plant Infection in
1070 *Fusarium graminearum*. *PLOS ONE* **7**:e49495.
1071 doi:10.1371/journal.pone.0049495
1072 Zhu T, Wang L, Rimbert H, Rodriguez JC, Deal KR, De Oliveira R, Choulet F,
1073 Keeble-Gagnère G, Tibbets J, Rogers J, Eversole K, Appels R, Gu YQ,
1074 Mascher M, Dvorak J, Luo M-C. 2021. Optical maps refine the bread wheat
1075 *Triticum aestivum* cv. Chinese Spring genome assembly. *Plant J* **107**:303–
1076 314. doi:10.1111/tpj.15289

1077

1078 **Funding**

1079 E.K and V.A are supported by the BBSRC-funded South West Biosciences Doctoral Training
1080 Partnership (BB/T008741/1). K.H.K and M.U are supported by the Biotechnology and
1081 Biological Sciences Research Council (BBSRC) Institute Strategic Programme (ISP) Grants,
1082 Designing Future Wheat (BBS/E/C/000I0250) and Delivering Sustainable Wheat
1083 (BB/X011003/1 and BBS/E/RH/230001B) and the BBSRC grants (BB/X012131/1 and
1084 BB/W007134/1). N.A.B was supported by the BBSRC Future Leader Fellowship
1085 BB/N011686/1. J.R and C.B are funded by the BBSRC ISPs Designing Future Wheat
1086 (BBS/E/C/000I0250), Delivering Sustainable Wheat (BB/X011003/1 and
1087 BBS/E/RH/230001B), and Growing Health (BB/X010953). R.A was supported by a
1088 BBSRC/EPSRC Interface Innovation Fellowship (EP/S001352/1).

1089 **Author's contributions**

1090 E.K conducted the experiments and wrote the manuscript. N.A.B, M.U, and K.H.K
1091 provided project oversight, experimental design and manuscript planning,
1092 development, and revisions. R.A helped with experimental design and data analysis.
1093 C.B and J.R generated ZtKnr4 mutant and completed associated characterisation

1094 experiments. A.M.U embedded, sectioned, and imaged samples for TEM analysis.

1095 V.A undertook the resin embedding, sectioning, and imaging.

1096

1097 **Competing interests**

1098 No competing interests declared.

1099 **Tables and Figures**

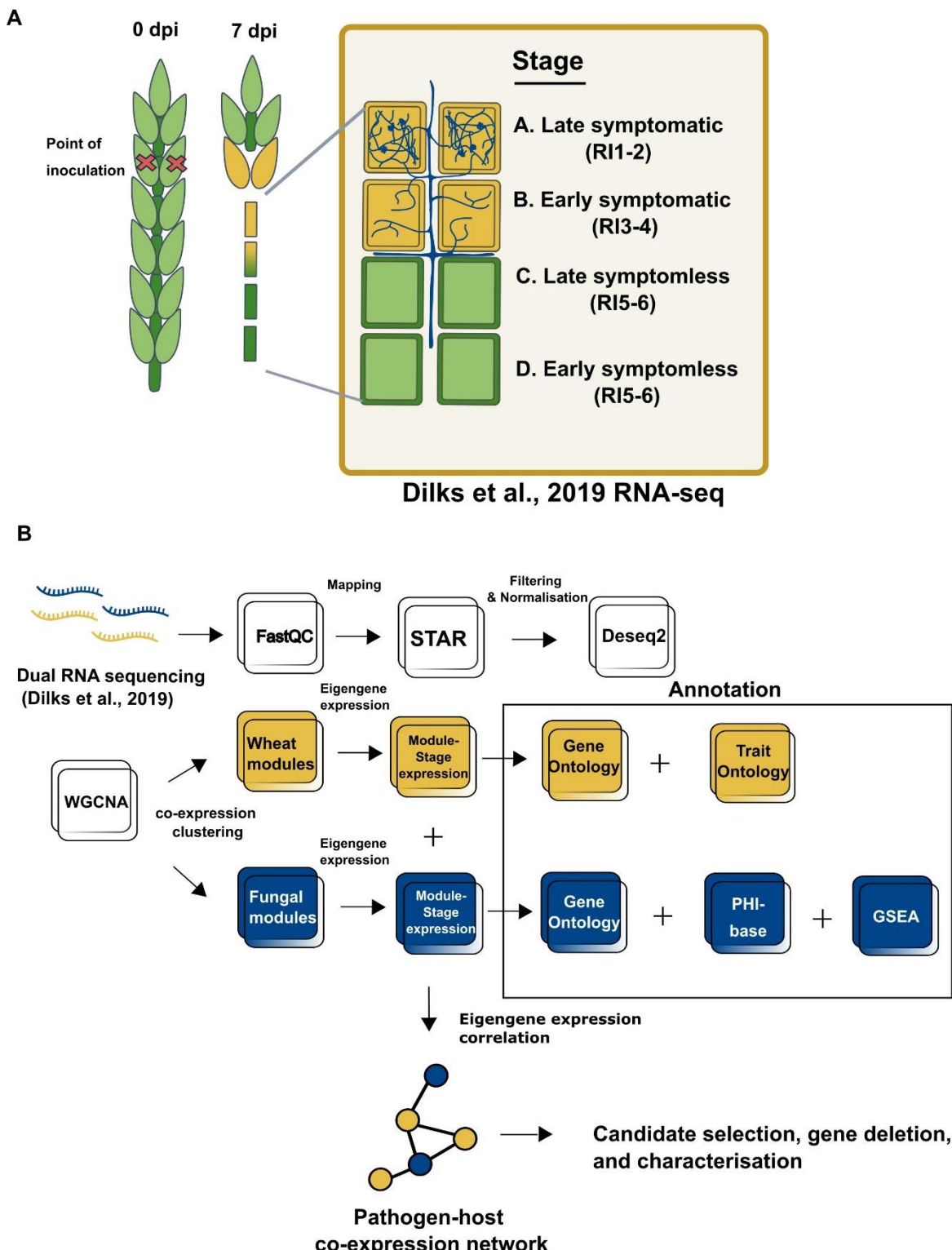
1100

1101 **Table 1. Function of correlated expression between wheat and fungal modules.** This table illustrates the relationship between wheat and
 1102 fungal gene expression at different stages of infection, detailing the associated functions and key fungal genes involved.

Expression Stages	Wheat Module	Predicted function	Correlated Fungal Module	Key Fungal Genes	Fungal Gene Functions	References	
Early symptomless stage of infection	W01	Maintenance genes (photosynthesis, RNA modification) and early defence response.	F16	<i>FgNPC1</i>	Regulation of membrane trafficking and sterol metabolism, which are essential for maintaining cellular integrity and function during the infection stages.	Breakspear et al. 2011	
				<i>Gzc2h045</i>	Msn2 C2H2 transcription factor, associated with virulence and coordination of adaptation to environmental stressors including heat, osmotic, and oxidative stress.	Son et al., 2011; John et al., 2021	
	W05	Disease resistance genes, including reactive oxygen species genes associated with programmed cell death response to restrict pathogen spread.		<i>GzCon7</i>	Msn2 C2H2 transcription factor, associated with virulence and regulation of cell wall biosynthesis.	Son et al., 2011; John et al., 2021	
				<i>FgSrp2</i>	Pre-mRNA processing, alternative splicing, and virulence	Zhang et al., 2020	

Early symptomless and late symptomatic stages of infection	W06	Enriched in protein catabolism and autophagy, involved in immune signalling, programmed cell death, and necrotrophic damage control.	F10	<i>KP4L-1, KP4L-2, KP4L-3</i>	Necessary for virulence, provide competitive advantage during new niche occupation, essential for intraspecific interactions at high fungal density	Lu and Faris, 2019; Vicente et al., 2022
				<i>FgOS-2, FgAtf-1</i>	Regulation of secondary metabolite production, sexual reproduction, and stress tolerance	Nguyen et al., 2013
				<i>FgHyd3, FgHyd5</i>	Attachment to hydrophobic surfaces, production of aerial mycelia	Shin et al., 2022
Late symptomless to early symptomatic	W12	Detoxification, response to toxic substances, and defence response.	F12	<i>TRI</i> genes (<i>TRI3, TRI4, TRI11, TRI12, TRI14</i>)	Production of DON mycotoxin needed for virulence.	Dyer et al., 2005; Kimura et al., 2007

1104

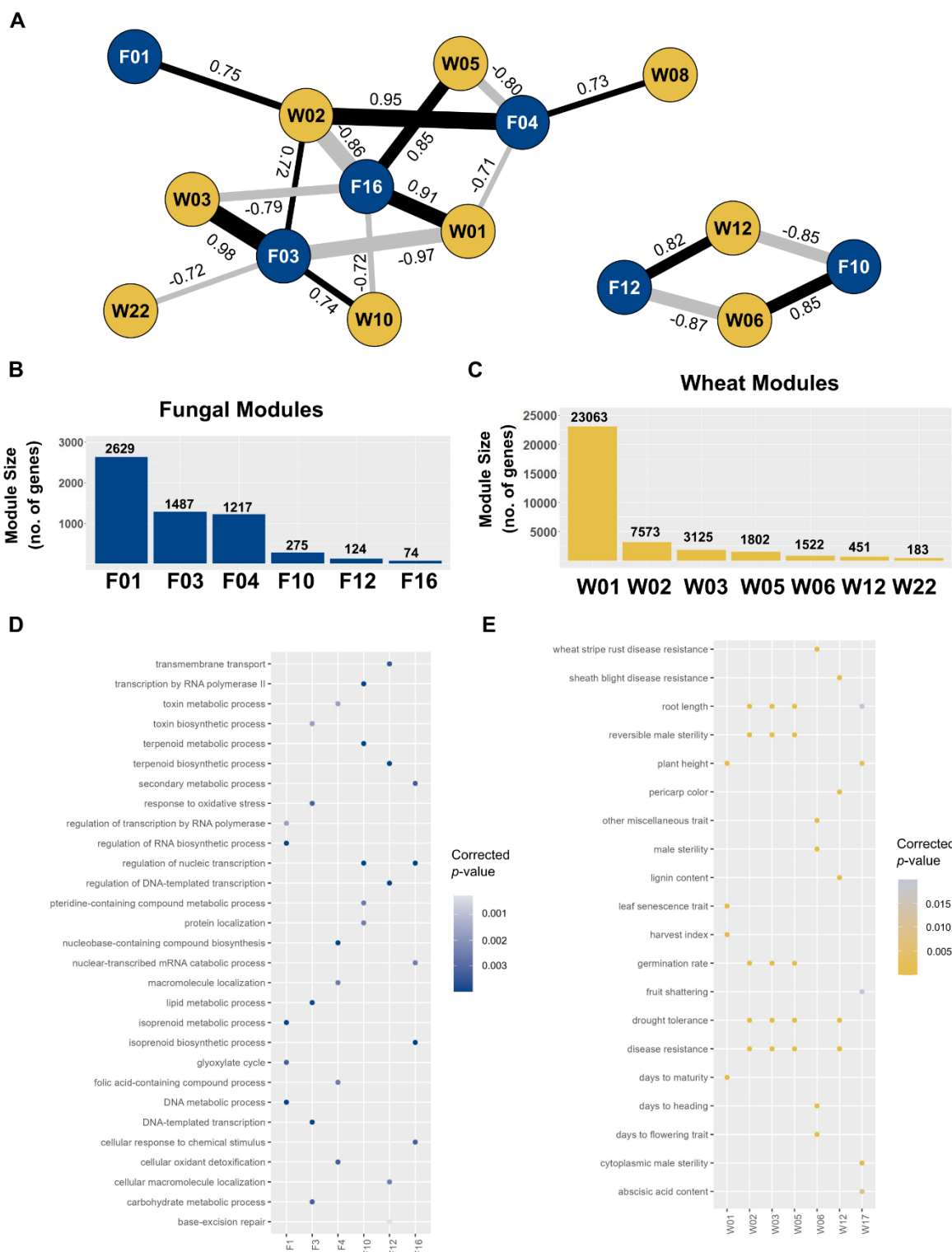


1105

1106 **Figure 1. Dual RNA-seq dataset and bioinformatics pipeline used for constructing the**
1107 **dual co-expression network. A.** Schematic illustration depicting the symptomatic (yellow)

1108 and symptomless (green) stages of *Fusarium graminearum* infection of wheat spikes
1109 denoted as stages A through D, corresponding to tissue samples collected for generating the
1110 RNA-seq data published in Dilks et al. 2019. *F. graminearum* hyphae growing in either the
1111 apoplast or inside the wheat cells are depicted in blue. **B.** Summary outlining the
1112 bioinformatics pipeline used for processing raw reads and constructing the dual RNA-seq
1113 network. The dual RNA-seq reads were initially processed together (processes depicted as
1114 white squares) before being separated to generate two distinct weighted gene co-expression
1115 networks. The bioinformatic pipelines are annotated accordingly, with yellow indicating the
1116 wheat reads-only pipeline and blue indicating the fungal reads-only pipeline. Annotation
1117 includes Gene Ontology terms (GO), Trait Ontology terms (TO), unique Gene Set
1118 Enrichment Analysis (GSEA), and PHI-base phenotypes. The modules from the two
1119 separate networks are then correlated to each other by their Eigengene values to form the
1120 dual co-expression network.

1121



1122

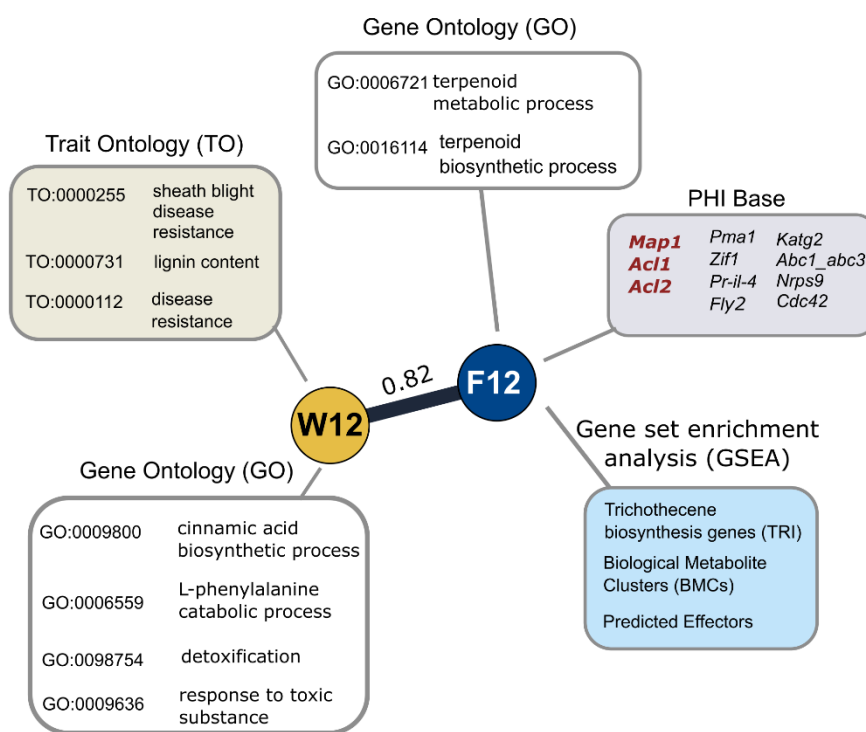
1123

1124 **Figure 2. Dual Fungal-Wheat co-expression network. A.** Network summarising significant
 1125 co-expression patterns ($p \geq 0.001$) between fungal modules (blue nodes) and wheat
 1126 modules (yellow nodes). Positive correlations are depicted as black edges, while negative

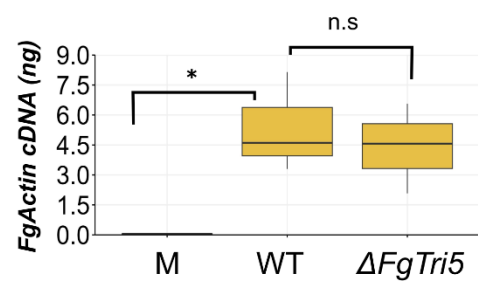
1127 correlations are shown as grey edges. R-squared values are indicated next to edges, with
1128 edge width corresponding to the value. **B. Fungal modules sizes. C. Wheat module sizes**
1129 (**Supplementary File 1**). **D. Fungal module enrichment.** Significant ($p \leq 0.05$) Biological
1130 Processes (BP) Gene Ontology (GO) enrichment results for all fungal modules in the
1131 network. Higher significance is indicated by darker blues. **E. Wheat module enrichment.**
1132 Significant Plant Trait Ontology (TO) enrichment results ($p \leq 0.05$) for all wheat modules in
1133 the network. Higher significance is indicated by brighter yellows.

1134

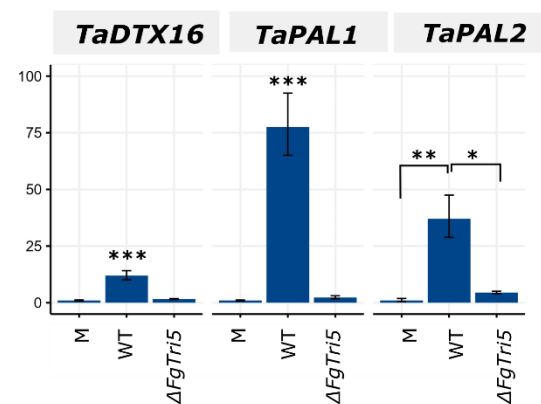
A



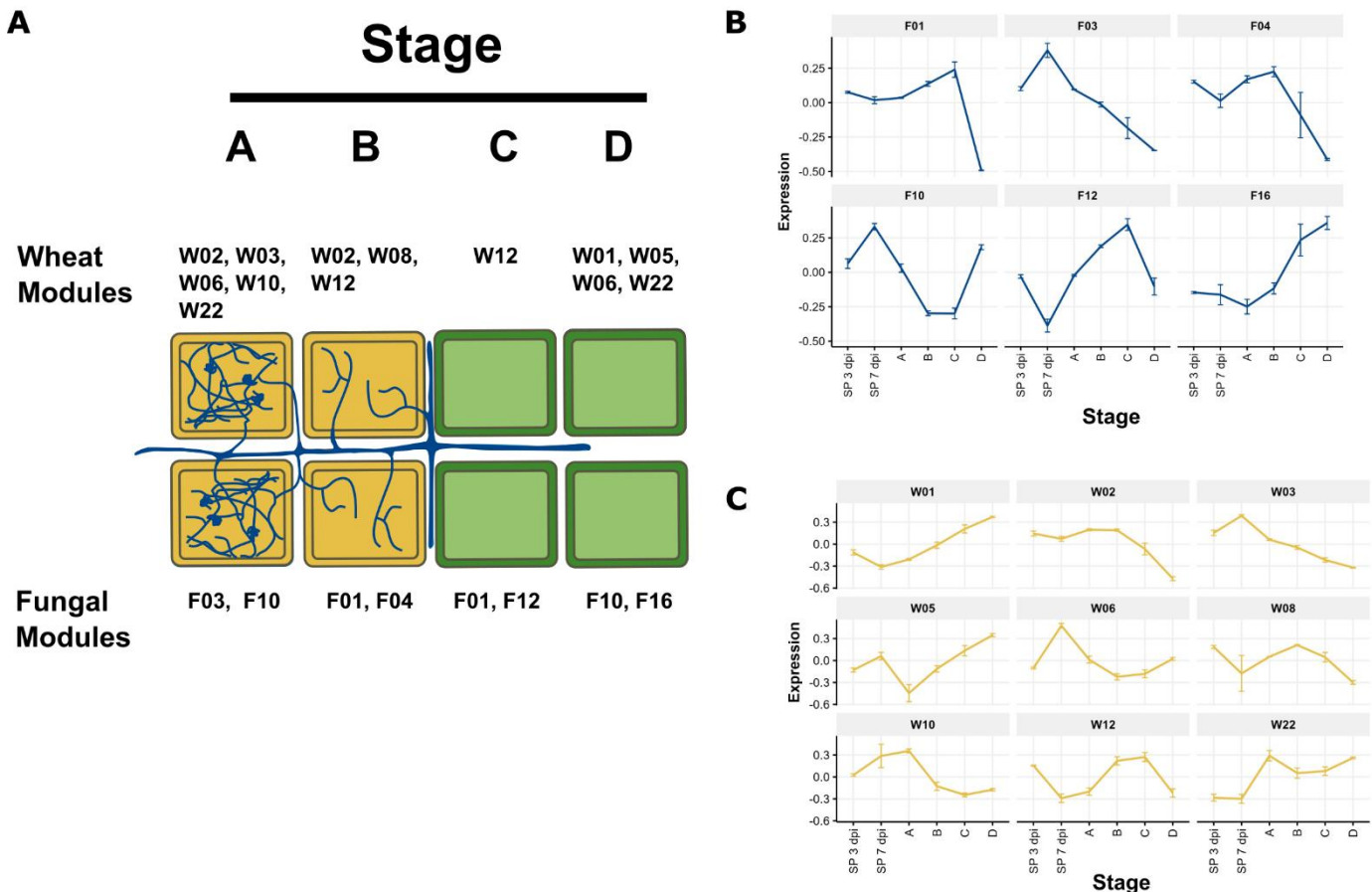
B



C



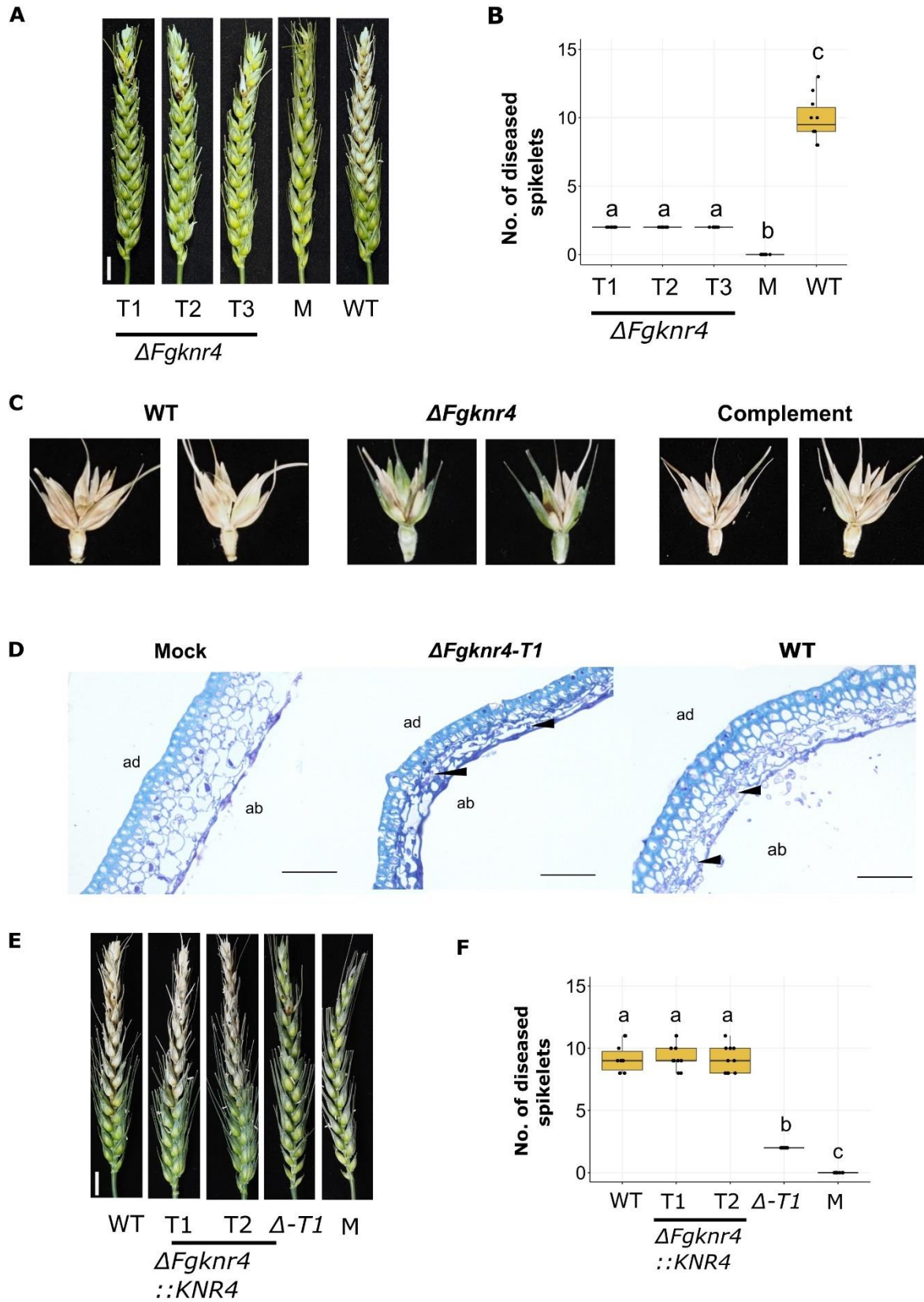
1135 **Figure 3. Validation of correlation between the trichothecene mycotoxin biosynthesis**
1136 **gene enriched module (F12) and the detoxification gene enriched module (W12). A.**
1137 Modules F12 (N = 124) and W12 (N = 451) depicted with significant enrichment annotations
1138 and genes with known phenotypes from PHI-base. Three genes listed in red in the PHI-base
1139 annotation (grey box) exhibit a loss of pathogenicity phenotype, while the remaining genes
1140 display a reduced virulence phenotype when individually deleted in *F. graminearum*. B.
1141 Equal levels of fungal burden were observed in tissue samples ($p > 0.05$). Absolute quantity
1142 of actin cDNA in Mock, $\Delta FgTri5$, and wild-type (WT)-recovered RI1-2 tissue sampled at 3 dpi.
1143 Significance was determined by a one-way ANOVA followed by Tukey HSD correction. C.
1144 Normalised fold change expression of selected W12 wheat genes in Mock, $\Delta FgTri5$, and WT-
1145 recovered RI1-2 tissue sampled at 3 dpi (N = 3). Significance is denoted as * = $p \leq 0.05$, ** =
1146 $p \leq 0.01$, and *** = $p \leq 0.001$. Significance was determined by a one-way ANOVA followed
1147 by Tukey HSD correction.



1148

1149 **Figure 4. Stage-specific expression of modules in the dual co-expression network. A.**
1150 Expression of modules across stages of *F. graminearum* infection. Illustration depicting
1151 symptomatic (yellow) and symptomless (green) stages of infection (A through D) annotated
1152 with specific modules (W or F) from the dual co-expression network that were highly
1153 expressed at specific stages **B. Eigengene summarised expression of fungal modules**
1154 and **C. wheat modules**. Eigengene summarised expression plots illustrating the expression
1155 patterns of genes in wheat modules across different stages of infection as illustrated in panel
1156 A, along with spikelet tissue (SP) at 3 and 7 dpi.

1157



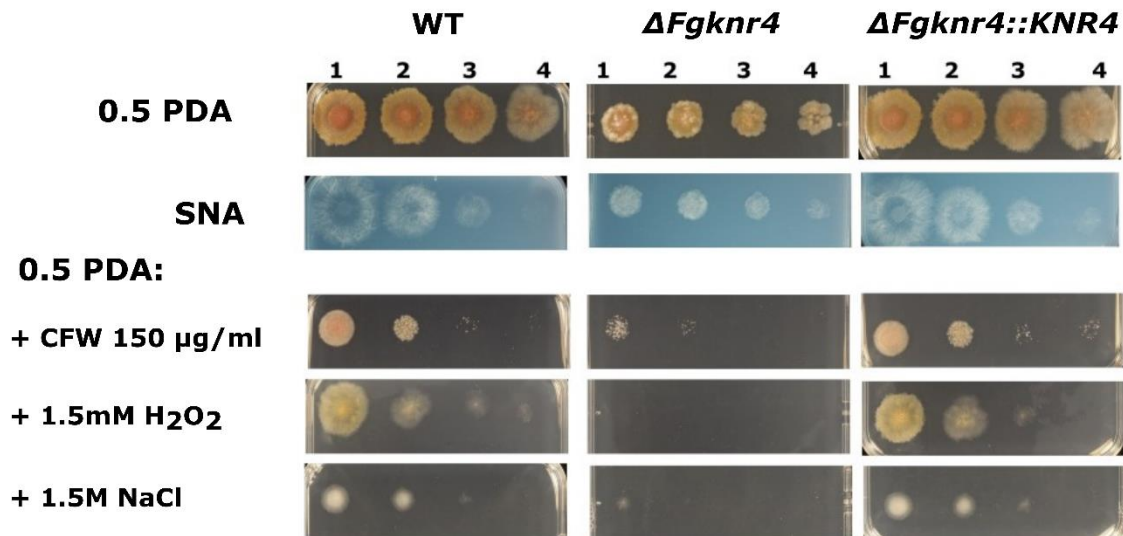
1160 **Figure 5. Decreased virulence observed during *in planta* infection with $\Delta Fgknr4$. A.**

1161 Wheat spike infection assay done on the susceptible cultivar Bobwhite point inoculated with
1162 sterile water only (Mock), wild-type *F. graminearum* conidia, or conidia from three
1163 independent single gene deletion *F. graminearum* mutants lacking *Knr4* ($\Delta Fgknr4$, T1-3).
1164 Images were captured at 15 dpi. Scale bar = 1 cm. **B.** Number of diseased spikelets per
1165 wheat spike at 15 dpi. Letters indicate significant differences (ANOVA, TukeyHSD $p < 0.05$).
1166 **C.** Symptom development on the inoculated spikelets and adjacent rachis tissues at 15 dpi
1167 **D.** Ultra-thin 1 μ m LR White resin sections stained with 0.1% Toluidine Blue for visualisation
1168 of wheat cell walls (light blue) and fungal hyphae (purple). Black arrows indicate fungal
1169 hyphae. Fungal hyphae typically proliferate in the abaxial cell layer. Ab = abaxial and ad =
1170 adaxial. Scale bar = 50 μ m. Tissue harvested at 7 dpi. **E.** Wheat spike infection
1171 complementation assay done on the susceptible cultivar Bobwhite treated with conidia either
1172 from wild-type *F. graminearum*, different complemented transformants ($\Delta Fgknr4::KNR4$ -T1
1173 and T2), the single gene deletion mutant ($\Delta Fgknr4$ -T1), or sterile water (mock). Images were
1174 taken at 15 days post inoculation. **F.** Number of diseased spikelets per wheat spike at 15
1175 dpi. Letters indicate significant differences (ANOVA, TukeyHSD $p < 0.05$).

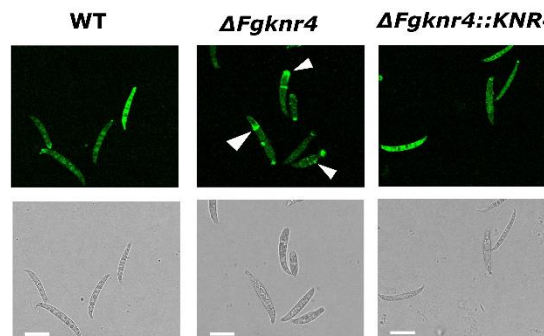
1176

1177

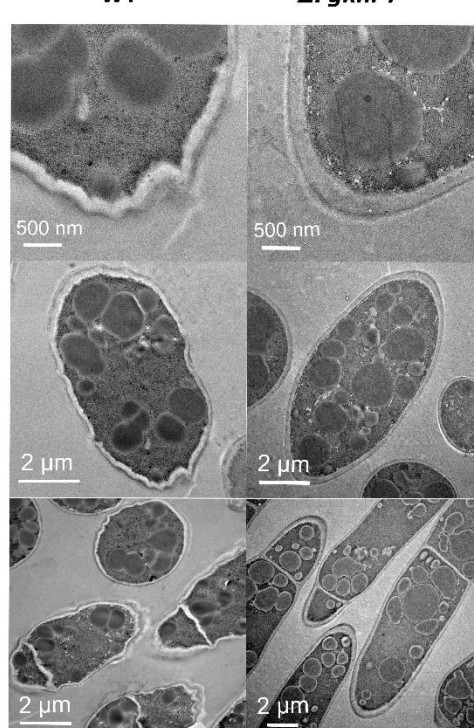
A



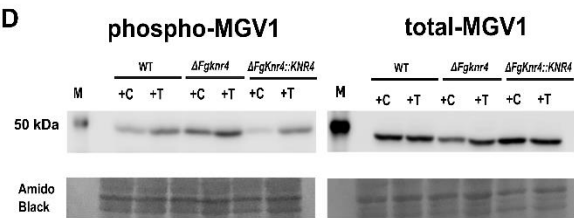
B



C



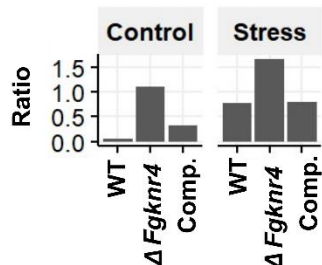
D



Legend: M Marker; C Control (Water); T Treatment (200 μ g/ml CFW)

E

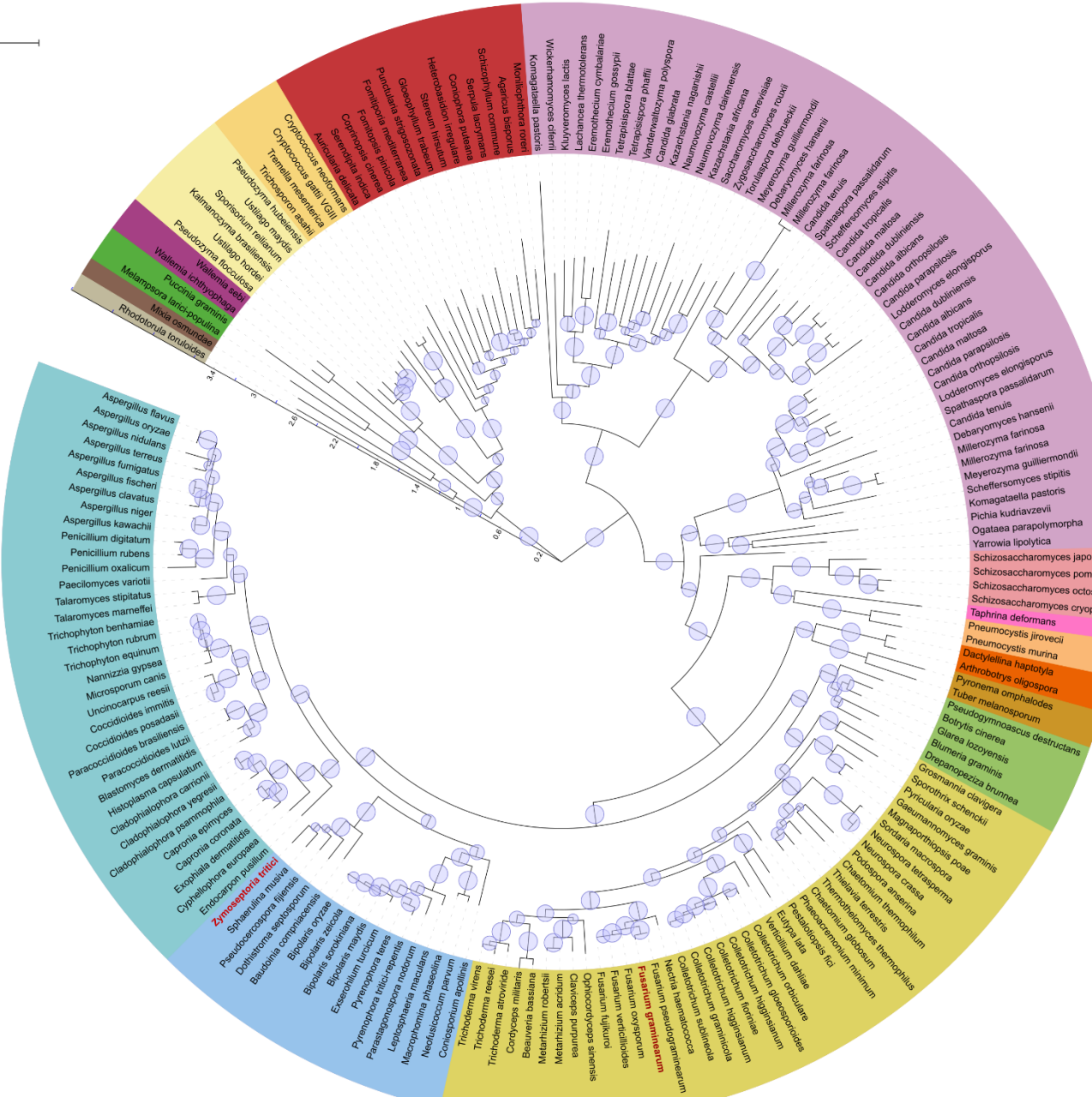
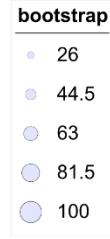
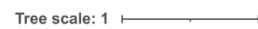
Phosphorylated MGV1:Total MGV1



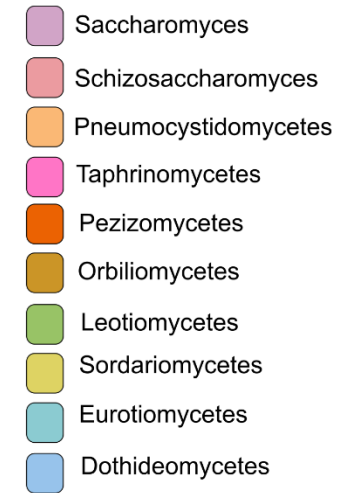
1178

1179 **Figure 6. Cell wall stress sensitivity and abnormal cell wall morphology of $\Delta Fgknr4$.** **A.**
1180 Dilution series of wild-type (WT), $\Delta Fgknr4$, and $\Delta Fgknr4::KNR4$ strains on Synthetic Nutrient
1181 Agar (SNA) and half-strength Potato Dextrose Agar (0.5 PDA) with and without the addition
1182 of calcofluor white (CFW), hydrogen peroxide (H_2O_2), and sodium chloride (NaCL). The
1183 dilution series begins at 1: 1 x 10^6 and continues with 10-fold dilutions (2: 1/10, 3: 1/100, and
1184 4: 1/100). Images taken after 3 days of growth at room temperature. **B.** Abnormal chitin
1185 deposition patterns in $\Delta Fgknr4$ conidia. Chitin-stained in conidia visualised using Wheat
1186 Germ Agglutinin Alexa Fluor™ 488 Conjugate (WGA). Scale bar = 50 μm . **C.** TEM imaging
1187 of wild-type and $\Delta Fgknr4$ conidia, showing differences in cell wall structure **D.** Western blot
1188 of proteins extracted from, $\Delta Fgknr4$ and $\Delta Fgknr4::KNR4$ mycelium incubated with (T) or
1189 without (C) the addition of 200 $\mu g/ml$ Calcofluor White (CFW) for 24 h. Phospho-p44/42
1190 MAPK (Erk1/2) and p44/42 MAPK (Erk1/2) antibodies were used to detect phosphorylated
1191 and total MGV1, respectively. Amido black total protein staining was performed to compare
1192 protein loading. **E.** Ratio of phosphorylated MAPK/total MAPK based on quantification of
1193 band intensity.

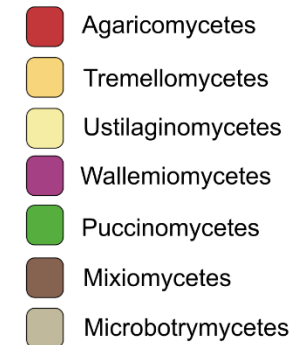
1194



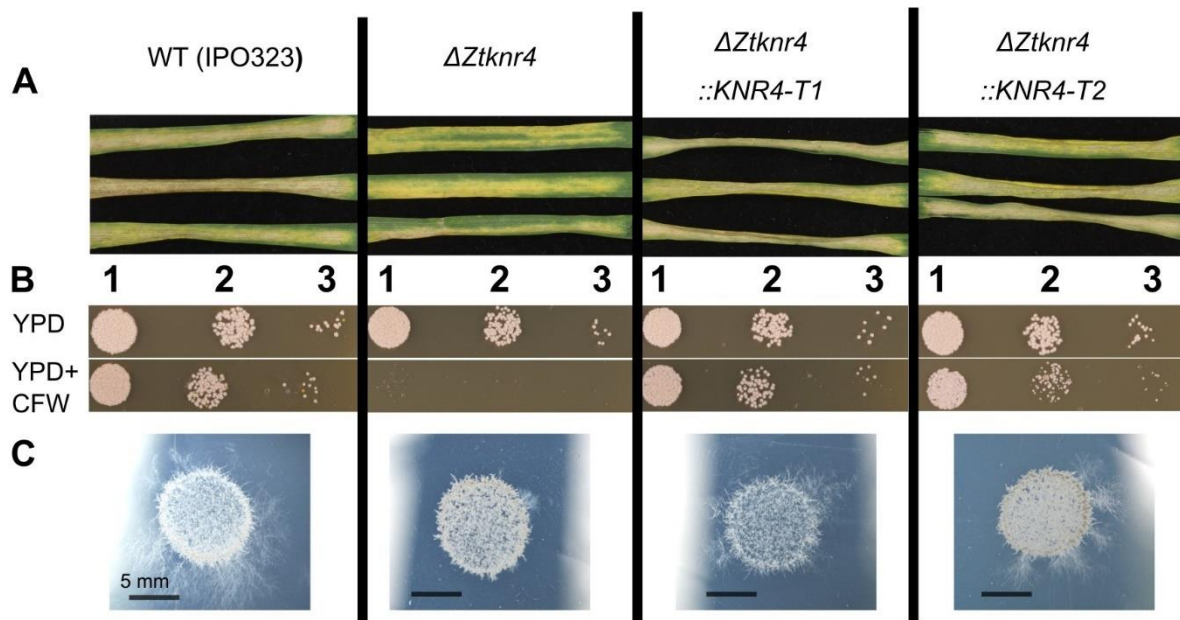
Ascomycota 82.2%



Basidiomycota 17.8%



1196 **Figure 7. Distribution of KNR4 orthologues across eukaryotes reveals exclusive presence in fungi.** A phylogenetic tree depicting the
1197 distribution of *KNR4* orthologues across Eukaryota, with the positions of *F. graminearum* and *Z. tritici* highlighted in red. Different taxonomic
1198 levels are indicated in various colours as specified in the legend, alongside the percent distribution of orthologues between Ascomycota and
1199 Basidiomycota. Evolutionary distances between species or taxa are denoted by an internal scale (range 0 - 3.5) Bootstrapping confidence
1200 values are depicted as pale blue circles, with increasing size corresponding to higher confidence levels.



1201

1202 **Figure 8. Functional characterisation of the *Zymoseptoria tritici* $\Delta Zt knr4$ gene**

1203 **deletion mutant. A.** Detached wheat leaves inoculated with wild-type (WT) *Z. tritici*
1204 (*IPO323*), $\Delta Zt knr4$ mutant strain, and two complemented strains ($\Delta Zt knr4::KNR4-T1$ and
1205 *T2*). Image taken at 20 dpi. **B** WT *Z. tritici*, the $\Delta Zt knr4$ mutant and two complemented
1206 strains ($\Delta Zt knr4::KNR4-T1$ and *T2*) spot inoculated onto YPD agar with (bottom) and
1207 without (top) calcofluor white (CFW). Dilution series begins at 1: 1 $\times 10^5$ and continues with
1208 10-fold dilutions (2: 1/10 and 3: 1/100). Images taken after 3 days of growth at room
1209 temperature (RT). **C** WT *Z. tritici*, the $\Delta Zt knr4$ mutant and two complemented strains
1210 ($\Delta Zt knr4::KNR4-T1$ and *T2*) spot inoculated onto 1% Tap Water Agar (TWA). Images taken
1211 after 10 days of growth at room temperature (RT).

A

Module	Module Size	GO MF/BP Summary	GO CC Summary	Trait Ontology (TO)
25	83	DNA integration	Cell periphery	ethylene sensitivity
24	96	Isopentenyl diphosphate biosynthesis	-	callus induction
23	153	Protein modification	-	other miscellaneous trait
22	183	-	-	other miscellaneous trait
21	199	-	-	total root number
20	235	DNA packaging	Nucleosome	cytoplasmic male sterility
19	254	Lipid biosynthesis and proteasome activity	Lipid droplet	cytoplasmic male sterility
18	287	Ubiquitination and protein catabolism	Proteosome complex	auxin sensitivity
17	316	Diterpenoid biosynthesis	Extracellular region	cytoplasmic male sterility
16	332	Protein phosphorylation and kinase activity	Integral component of membrane	disease resistance
15	334	Fatty acid metabolism and synthesis	-	plant height
14	374	Translation	Cytosolic ribosome	stem elongation
13	379	Structural constituent of ribosome	Cytosolic ribosome	leaf senescence trait
12	451	Detoxification and response to toxic substance	-	sheath blight disease resistance
11	501	Glycolysis	-	self-incompatibility
10	695	Protein localisation and autophagy	Protein-containing complex	male sterility
9	765	Protein phosphorylation and kinase activity	Integral component of membrane	germination rate
8	818	Protein phosphorylation and defense response	Integral component of membrane	disease resistance
7	1544	Response to water and water channel activity	Chloroplast	cold tolerance
6	1552	Protein catabolism and autophagy	Proteosome complex	days to flowering trait
5	1802	Vesicle transport and hydrolase activity	Vesicle	disease resistance
4	2344	Gene expression	Ribonucleoprotein complex	disease resistance
3	3125	Proteolysis and autophagy	Peroxisome	disease resistance
2	7573	Gluthathione metabolism and response to biotic stimuli	Extracellular region	disease resistance
1	23063	RNA modification and defense response	Chloroplast	harvest index

B

Module	Module size	Phenotype				GO MF/BP Summary	GO CC Summary	Gene set enrichment
		LOP	RV	L	U			
18	60	0	0	0	3	-	-	
17	62	0	0	0	3	-	-	
16	74	0	4	0	2	-	-	
15	75	0	0	0	2	-	-	
14	79	0	2	1	3	-	-	
13	121	0	2	0	6	-	-	
12	124	3	11	0	6	Terpenoid metabolic process	Extracellular region	
11	253	0	6	1	15	-	-	
10	275	0	11	0	14	-	-	
9	353	1	13	5	25	-	-	
8	406	0	10	1	9	-	-	
7	442	0	0	0	1	Translation	Cytoplasm	
6	607	0	9	3	35	-	-	
5	647	2	43	13	26	Metabolic processes	Cytoplasm	
4	1217	1	9	6	88	Transcription factor activity	Ribosome	
3	1278	0	6	1	77	Oxidoreductase activity	Membrane	
2	1487	4	66	12	88	Cellular Organisation	Membrane	
1	2629	4	65	16	184	Transcription factor activity	Nucleus	

1212

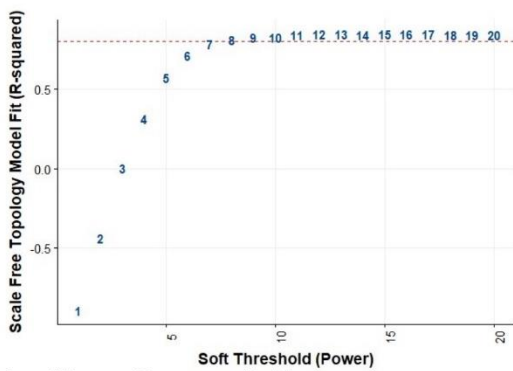
1213 **Figure 2 – figure supplement 1. Network Summary.** A. Summary of all modules in the
 1214 wheat network, including module size (number of genes), Gene Ontology (GO) and Trait
 1215 Ontology (TO) enrichment summaries. B. Summary of all modules in the fungal network,
 1216 including modules size, Gene Ontology (GO) enrichment summaries and Gene Set

1217 Enrichment Analysis (GSEA). The number of genes with different phenotypes in PHI-base
1218 are depicted, with LOP, RV, L and U denoting different PHI-base phenotypes (LOP = Loss of
1219 pathogenicity; RV = Reduced virulence; L = Lethal; U = Unaffected pathogenicity) (**Urban et**
1220 **al., 2022**).

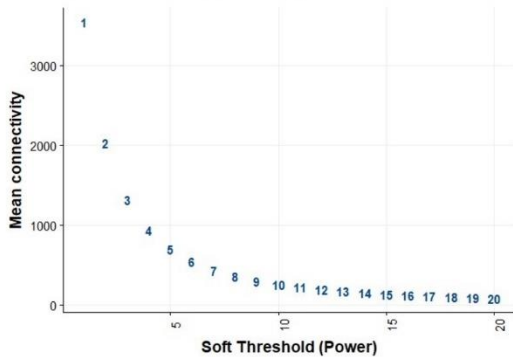
1221

Fungal

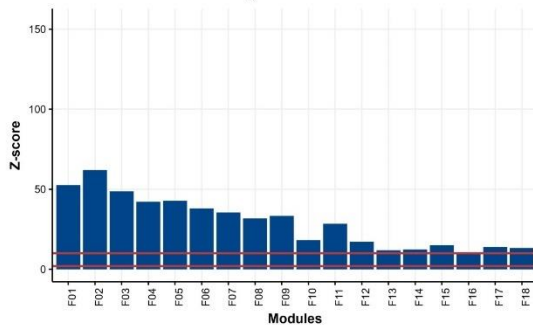
A. Scale Free Model Fit



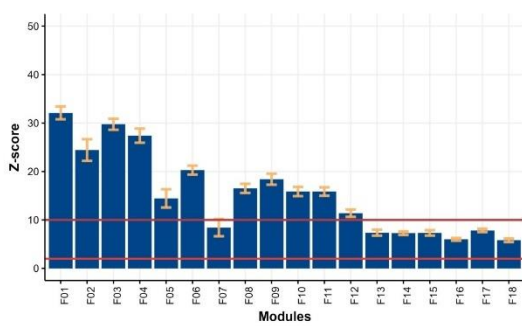
B. Mean Connectivity



C. Module Quality

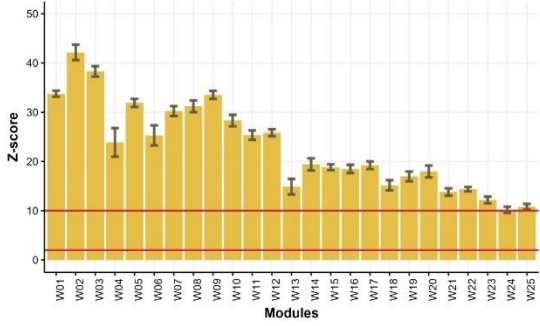
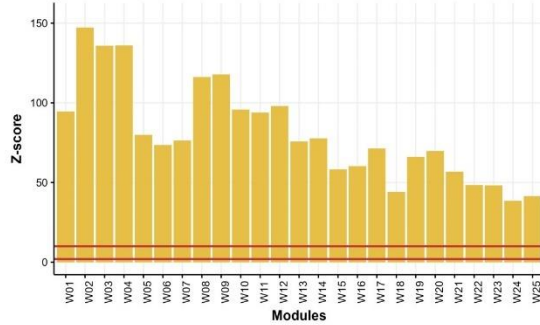
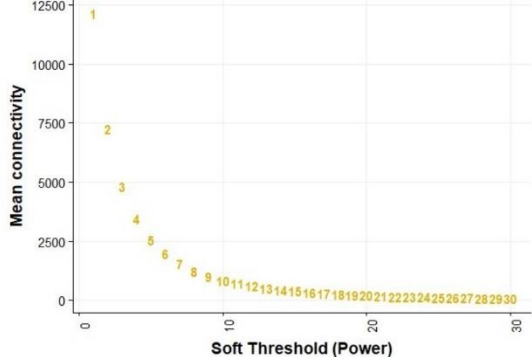
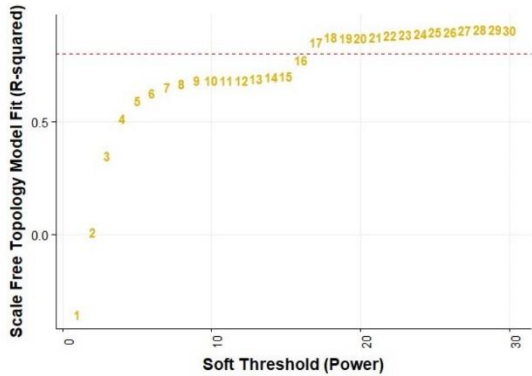


D. Module Preservation



Wheat

A. Scale Free Model Fit



1222

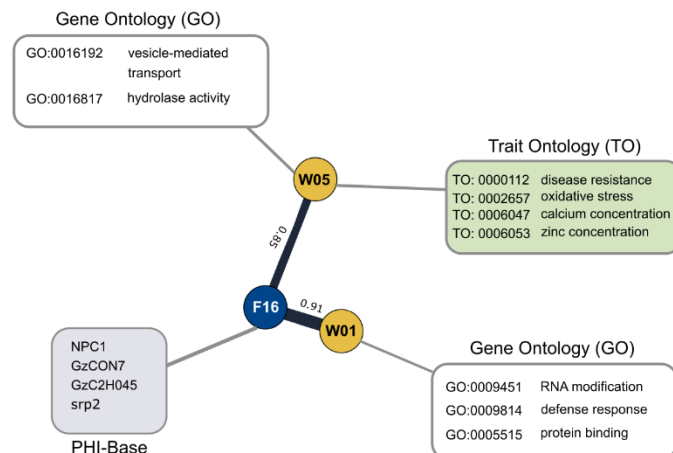
1223 **Figure 2 – figure supplement 2. Network statistics. A.** Strength of correlation of network

1224 model (R-squared value) to scale free model at different soft thresholding powers. Dotted

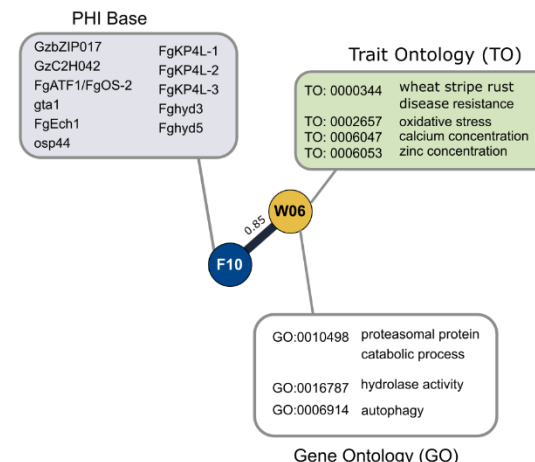
1225 red line is at an R-squared value of 0.80, the threshold needed for generating a WGCNA
1226 network. **B.** Mean connectivity of genes in each network at different soft thresholding
1227 powers. A low mean connectivity is desired to meet the scale free network criteria. **C.**
1228 Module quality across all modules as determined by a Z-score calculation. Solid red lines at
1229 minimum quality ($Z = 2$) and high quality scores ($Z = 10$). **D.** Module preservation as
1230 determined by Z-score calculation against 50 random test networks. Solid red lines at
1231 minimum preservation ($Z = 2$) and high preservation scores ($Z = 10$).

1232

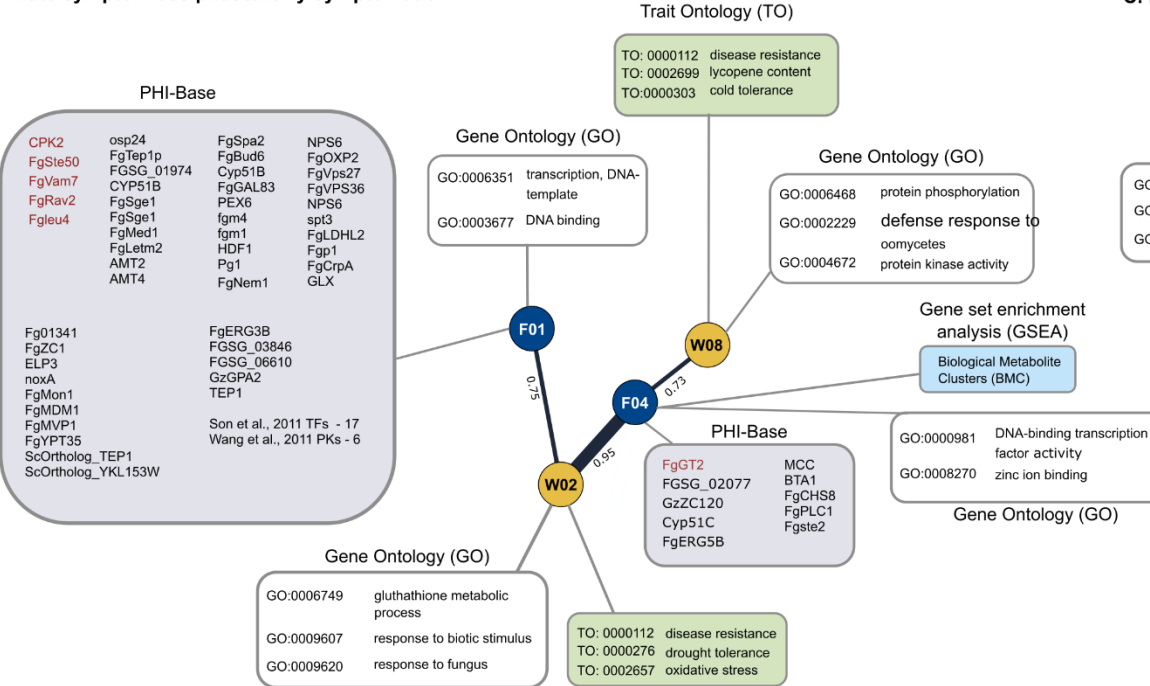
A. Early symptomless phase



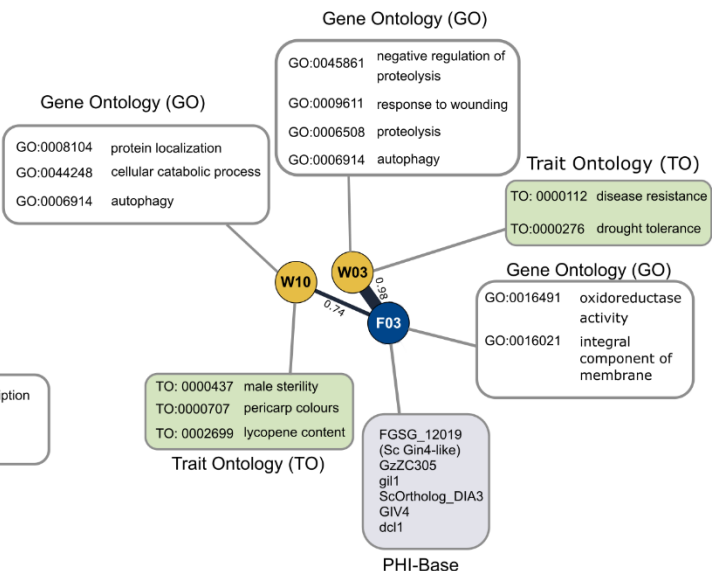
B. Early symptomless and late symptomatic



B. Late symptomless phase/Early symptomatic

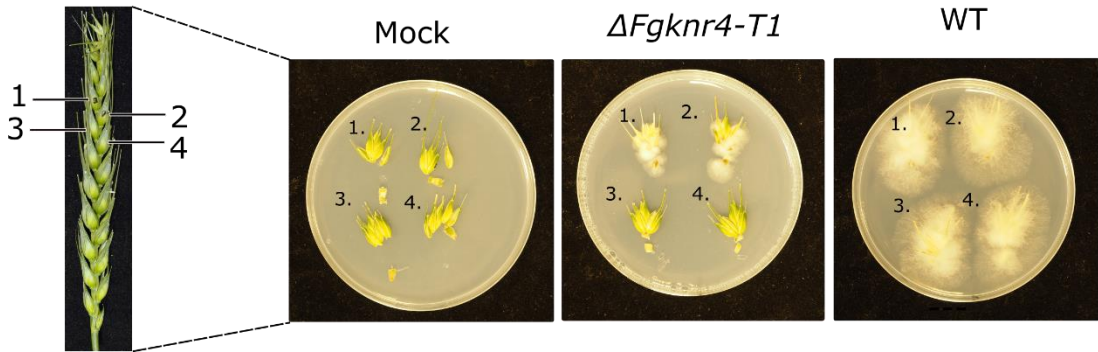


C. Late symptomatic phase



1234 **Figure 4 – figure supplement 1. Annotation of stage-specific modules.** Fungal modules (F) and wheat modules (W) depicted with
1235 significant enrichment annotations. Fungal modules are additionally annotated with known phenotypes from PHI-base. Genes listed in red in
1236 the PHI-base annotation (grey box) exhibit a loss of pathogenicity phenotype when deleted, while the remaining genes display a reduced
1237 virulence phenotype when deleted. Plots are separated by modules with highest expression in a given stage of infection, namely **A. Early**
1238 **symptomless, B. Early symptomless and late symptomatic, C. Late symptomless/Early symptomatic, and D. Late symptomatic.**

1239



1240

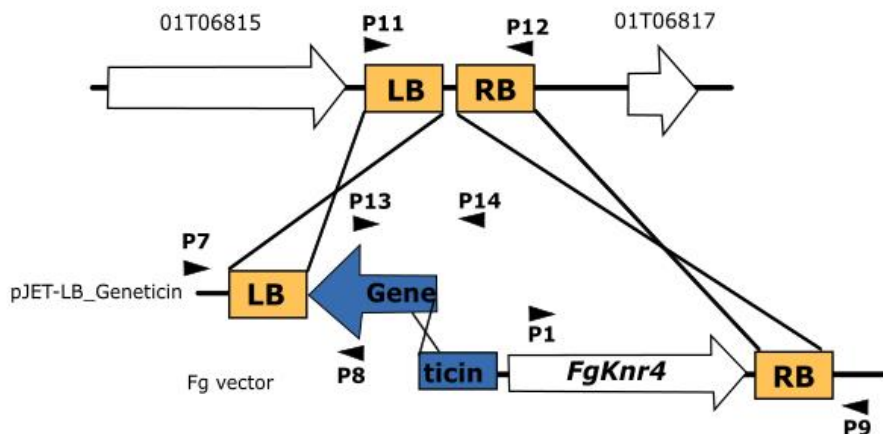
1241 **Figure 5 – supplement 1. Surface sterilisation of dissected wheat floral tissue. .**

1242 Dissection at 15 dpi of wheat spikes followed by separation of infected wheat spikelet and

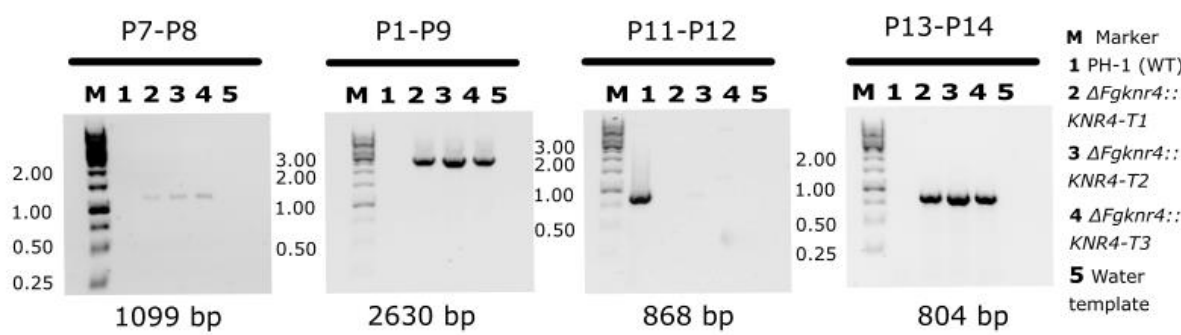
1243 rachis tissues and subsequent plating onto synthetic nutrient agar (SNA) separated at 15

1244 dpi. Plate images taken 3 days later.

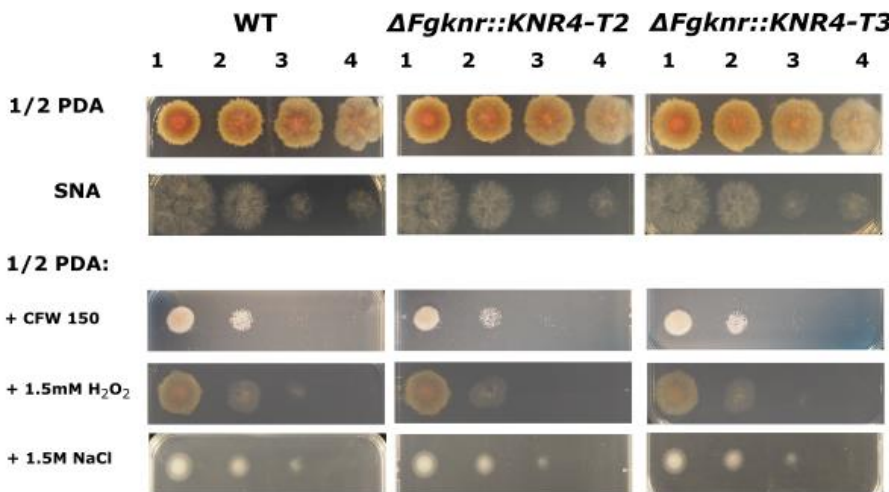
A



B



C



1245

1246 **Figure 6 – figure supplement 1. *FgKnr4* single gene deletion strategy and**

1247 **characterisation of additional transformants. A.** Schematic for the hygromycin split

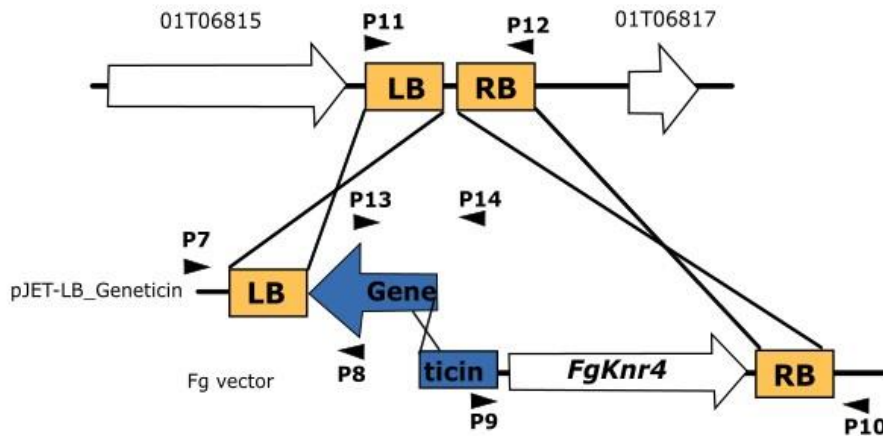
1248 marker deletion strategy including diagnostic primer locations (P1-6). **B.** Diagnostic PCR

1249 with primer sets depicted in panel A. PCR samples were separated on 7.5 % agarose gel
1250 with a 1 kb DNA ladder. The expected amplicon size is written below the corresponding gel
1251 image. **C.** Dilution series of wild-type (WT) and additional $\Delta Fgknr4$ transformants (*T2* and
1252 *T3*) on Synthetic Nutrient Agar (SNA) and half-strength Potato Dextrose Agar (0.5 PDA) with
1253 and without the addition of single stresses. The dilution series begins at 1: 1 $\times 10^6$ and
1254 continues with 10-fold dilutions (2: 1/10, 3: 1/100, and 4: 1/100). Images taken after 3 days.

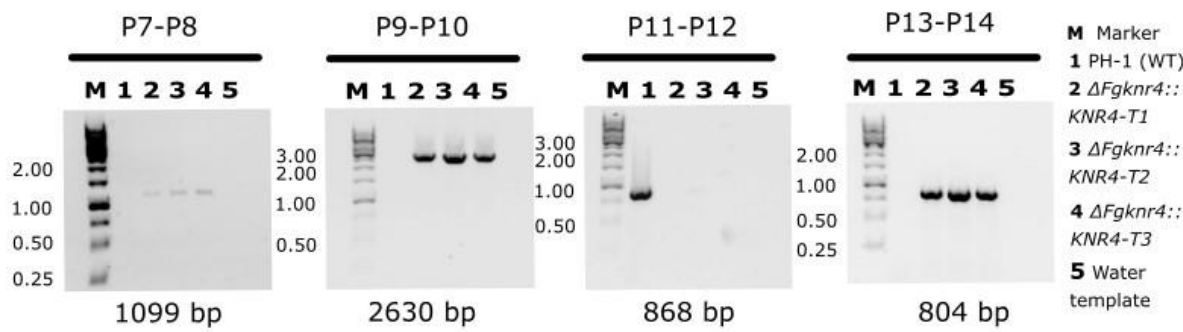
1255

1256

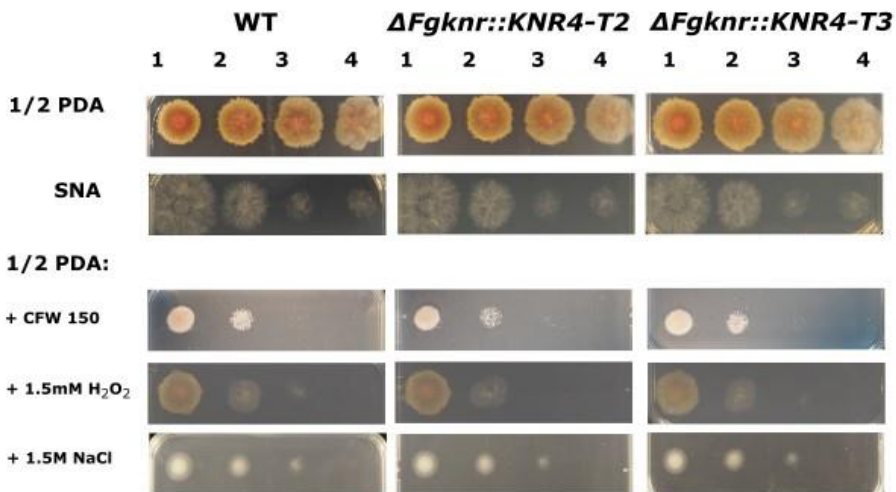
A



B



C

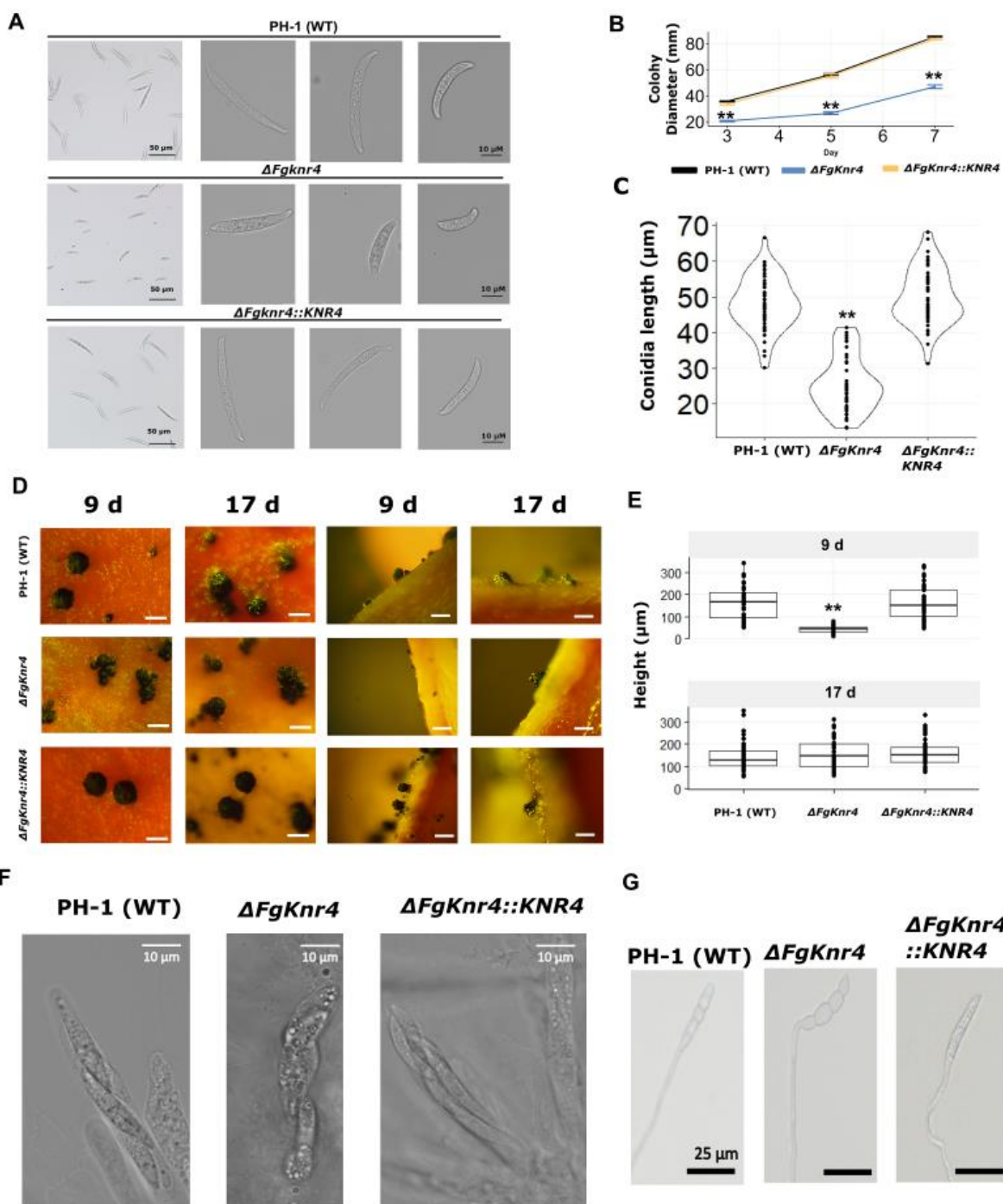


1257

1258 **Figure 6 – figure supplement 2. $\Delta Fgknr4-T1$ complementation strategy and**
1259 **characterisation of additional transformants. A.** Schematic of gene complementation into
1260 the *Fg* transformation locus (Diarino et al. (2024), including diagnostic primer locations (P7-

1261 P14). **B.** Diagnostic PCR with primer sets depicted in panel A. PCR samples were separated
1262 on 7.5 % agarose gel with a 1 kb DNA ladder. Expected amplicon size is written below the
1263 corresponding gel image. **C.** Dilution series of wild-type (WT) and additional $\Delta Fgknr4::KNR4$
1264 transformants ($T2$ and $T3$) on Synthetic Nutrient Agar (SNA) and half-strength Potato
1265 Dextrose Agar (0.5 PDA) with and without the addition of single stresses. The dilution series
1266 begins at 1: 1 $\times 10^6$ and continues with 10-fold dilutions (2: 1/10, 3: 1/100, and 4: 1/100).
1267 Image taken after 3 days.

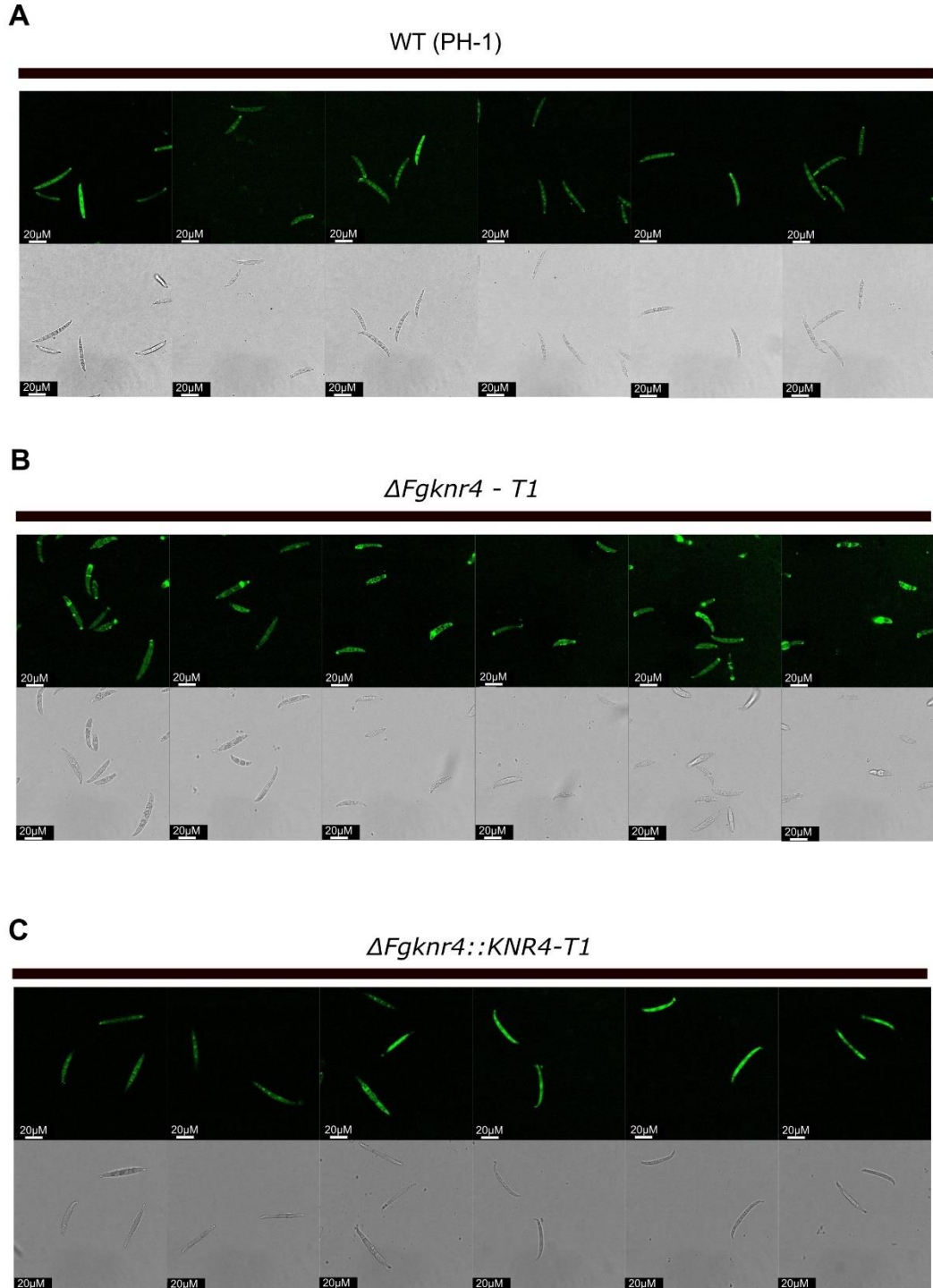
1268



1269

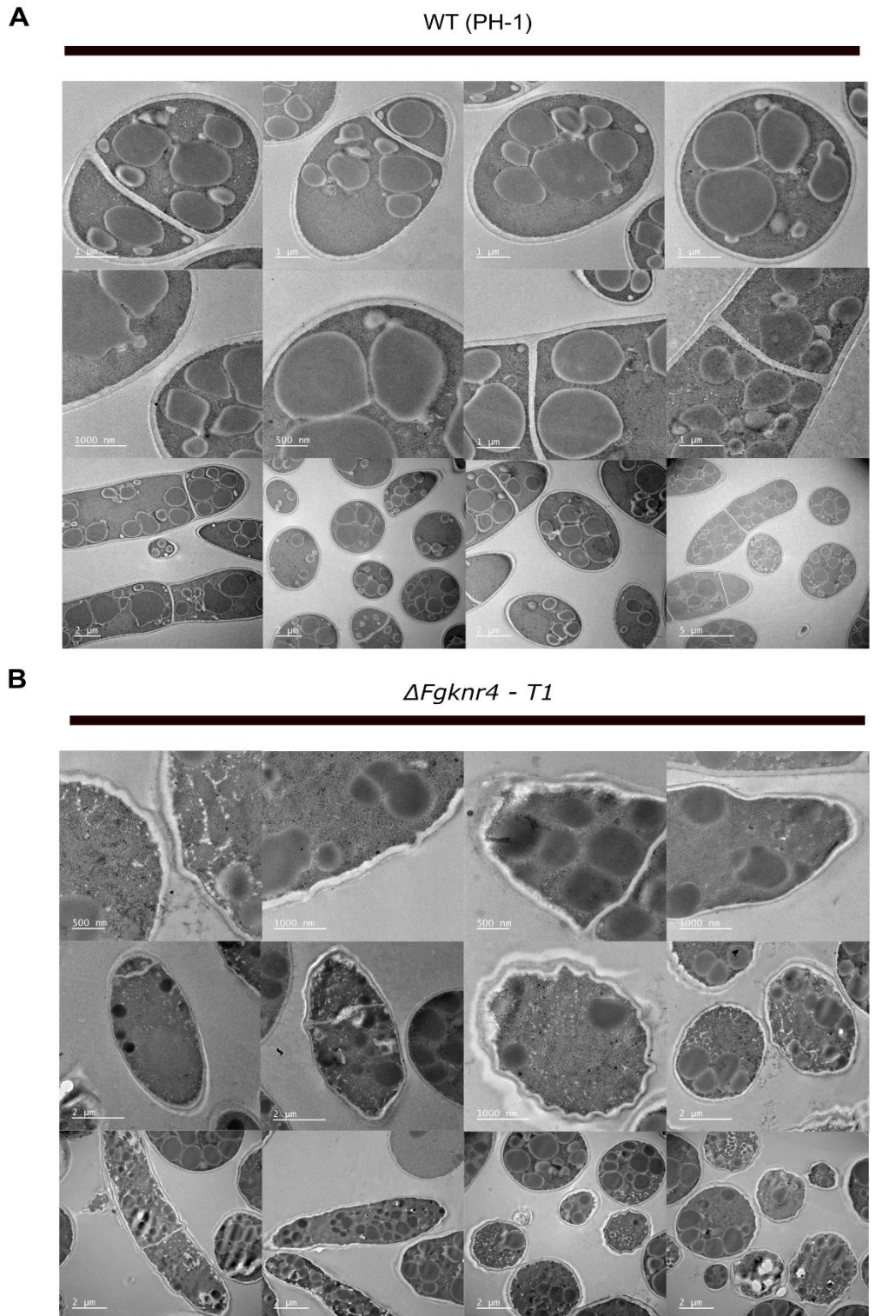
1270 **Figure 6 – figure supplement 3.** Characterisation of growth rate, conidial size and
1271 ascospore production in $\Delta Fgknr4$ and complemented strains. A. Decreased conidial size
1272 observed in $\Delta Fgknr4$. Single conidial images to represent long, middle length, and short
1273 conidia across strains. B. Mean colony diameter of wild-type (WT), $\Delta Fgknr4$, and
1274 $\Delta Fgknr4::KNR4$ grown on Potato Dextrose Agar (PDA) (N=5). C. Distribution of conidial

1275 length from N = 50 spores for wild-type (WT), $\Delta Fgknr4$, and $\Delta Fgknr4::KNR4$ strains. D.
1276 Representative perithecia images taken after perithecia induction in carrot agar medium
1277 using wild-type (WT), $\Delta Fgknr4$, and $\Delta Fgknr4::KNR4$ strains. Images taken from above (left
1278 panels) and from agar sections placed on slides (right panels) on day 9 and day 17. Scale
1279 bar = 500 μ m. F. Ascospores in intact ascus produced by wild-type (WT), $\Delta Fgknr4$ or
1280 $\Delta Fgknr4::KNR4$ strains. Scale bar = 10 μ M. G. Ascospores obtained from squashed
1281 perithecia of wild-type (WT), $\Delta Fgknr4$ or $\Delta Fgknr4::KNR4$ strains are viable and form germ
1282 tubes. Scale bar = 25 μ m. Significance is denoted as **= $p \leq 0.01$. Significance was
1283 determined by a one-way ANOVA followed by Tukey HSD correction.



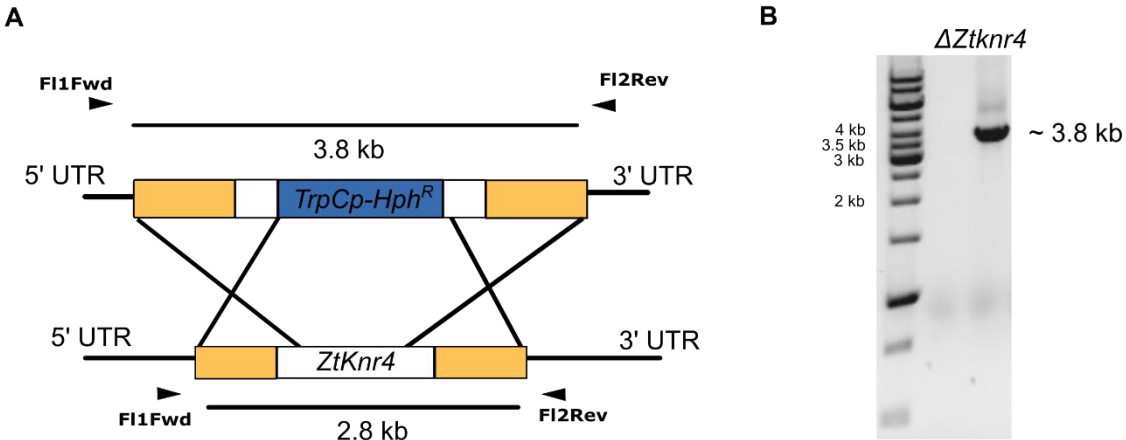
1284

1285 **Supplementary Figure 6 – figure supplement 4. Additional fluorescent microscopy**
1286 **images of irregular chitin distribution in $\Delta Fgknr4$ conidia**. Visualisation of chitin-stained
1287 conidia with Wheat Germ Agglutinin Alexa Fluor™ 488 Conjugate (WGA) in wild-type (WT)
1288 (A), $\Delta Fgknr4$ (B) and $\Delta Fgknr4::KNR4$ (C).



1289

1290 **Figure 6 – figure supplement 5. Additional TEM images of abnormal cell wall**
1291 **morphology in $\Delta Fgknr4$ conidia.** TEM imaging of wild-type (A) and $\Delta Fgknr4$ (B) conidia,
1292 showing differences in cell wall structure and different magnifications.



1293

1294 **Figure 8 – figure supplement 1.** $\Delta Ztknr4$ diagnostic PCR and disruption deletion strategy.

1295 **A.** Hygromycin (Hph^R) replacement cassette inserts at $ZtKnr4$ locus through homologues
1296 recombination via homologous flanks (yellow and white). **B.** Diagnostic PCR demonstrating
1297 presence of large insertion fragment in $\Delta ZtKnr4$ transformant using F11Fwd and F12Rev
1298 primers.

1299 **Supplementary File 1. Network module sizes and gene module assignments.**
1300 Spreadsheet containing sizes of all modules in fungal and wheat networks. 'Fungal module
1301 assignments' and 'Wheat module assignments' tabs contain a column with all fungal IDs
1302 (RRES v.5 PH-1) or wheat IDs (Column A = IWGSC RefSeq v2.1; Column B = IWGSC
1303 RefSeq v1.1) with an adjacent column denoting which module they are clustered in.
1304 **Supplementary File 2. *F. graminearum* genes with known phenotypes with the PHI-base**
1305 [database \(\[www.PHI-base.org\]\(http://www.PHI-base.org\)\)](http://www.PHI-base.org) in each fungal module. Table provides RRES v5 gene ID,
1306 PHI identifier ID from PHI-base, Uniprot protein ID, gene function, mutant phenotype, author
1307 reference, and year published.
1308 **Supplementary File 3. Primer list.** Primers used to generate mutant and complemented
1309 strains.
1310
1311

1312 **Table S1. Candidate gene selection in fungal module F16.** Table provides details on the 15 candidates within module F16 with the highest
 1313 module membership (MM) and reason for exclusion from further functional characterisation analysis. This table includes the MM score and
 1314 associated *p*-values (p.MM), as well as correlation strength to corresponding wheat modules (Cor) and *p*-values (p.Cor).

ID	COR.W05	P.COR.W0	GS.W01	P.COR.W01	MM.F16	P.MM.F16	INTERPRO DESCRIPTION	REASON
							5	FOR EXCLUSION
FGRAMPH1_01T20453	0.79	0.00	0.93	0.00	0.95	0.00	N/A	Unknown domain
FGRAMPH1_01T06173	0.88	0.00	0.77	0.00	0.94	0.00	domain of unknown function DUF2405;	Unknown domain
FGRAMPH1_01T22959	0.69	0.00	0.94	0.00	0.93	0.00	RNA recognition motif domain;U1 small nuclear ribonucleoprotein of 70kDa N-terminal;snRNP70, RNA recognition motif;RNA-binding domain superfamily;U1 small nuclear ribonucleoprotein 70kDa	75 genes with this domain in <i>F. graminearum</i> proteome

FGRAMPH1_01T10513	0.73	0.00	0.76	0.00	0.91	0.00	Helicase, C-terminal;DEAD/DEAH box helicase domain;Helicase superfamily 1/2, ATP-binding domain;P-loop containing nucleoside triphosphate hydrolase	26 ancient paralogues on Ensembl (2022)
FGRAMPH1_01T00861	0.86	0.00	0.76	0.00	0.91	0.00	BRCT domain;AAA+ ATPase domain;ATPase, AAA-type, core;DNA polymerase III, clamp loader complex, gamma/delta/delta subunit, C-terminal;Replication factor C subunit 1;DNA replication factor RFC1, C-terminal;P-loop containing nucleoside triphosphate hydrolase;BRCT domain superfamily	2 ancient paralogues on Ensembl (2022)
FGRAMPH1_01T00671	0.69	0.00	0.80	0.00	0.91	0.00	PAP/25A-associated;Nucleotidyltransferase superfamily	1 ancient parologue on Ensembl (2022)

FGRAMPH1_01T00977	0.83	0.00	0.85	0.00	0.90	0.00	Endoplasmic reticulum vesicle transporter, C-terminal;Endoplasmic reticulum vesicle transporter, N-terminal	1 ancient parologue on Ensembl (2022)
FGRAMPH1_01T18141	0.72	0.00	0.83	0.00	0.90	0.00	CDC48, N-terminal subdomain;AAA+ ATPase domain;ATPase, AAA-type, core;ATPase, AAA-type, conserved site;CDC48, domain 2;Aspartate decarboxylase-like domain superfamily;Vps4 oligomerisation, C-terminal;P-loop containing nucleoside triphosphate hydrolase;CDC48 domain 2-like superfamily;AAA ATPase, AAA+ lid domain	15 ancient paralogues on Ensembl(202 2)

FGRAMPH1_01T22333	0.83	0.00	0.75	0.00	0.90	0.00	AMP-dependent synthetase/ligase;Phosphopantetheine binding ACP domain;Trimeric LpxA-like superfamily;Polyketide synthase, phosphopantetheine-binding domain;ACP-like superfamily	BLAST hit in <i>F. graminearum</i> PH-1 genome (E = 4.5e-063)
FGRAMPH1_01T27545	0.71	0.00	0.88	0.00	0.90	0.00	Sterol-sensing domain;Protein patched/dispatched;Niemann-Pick C1, N-terminal	Previously studied. Reduced virulence phenotype (Breakspear et al. 2011)
FGRAMPH1_01T23707	0.82	0.00	0.74	0.00	0.90	0.00	Knr4/Smi1 family;Knr4/Smi1-like domain	
FGRAMPH1_01T27219	0.66	0.00	0.93	0.00	0.89	0.00	N/A	Unknown domain

FGRAMPH1_01T02111	0.81	0.00	0.85	0.00	0.89	0.00	DNA-directed RNA polymerase, subunit 2, hybrid-binding domain;RNA polymerase, beta subunit, conserved site;RNA polymerase Rpb2, domain 7;RNA polymerase Rpb2, domain 2;RNA polymerase, beta subunit, protrusion;RNA polymerase Rpb2, domain 3;RNA polymerase Rpb2, domain 4;RNA polymerase Rpb2, domain 5;DNA-directed RNA polymerase, subunit 2	2 ancient paralogues on Ensembl (2022)
FGRAMPH1_01T04893	0.75	0.00	0.69	0.00	0.88	0.00	SNF2-related, N-terminal domain;Helicase, C-terminal;Helicase superfamily 1/2, ATP-binding domain;DBINO domain;P-loop containing nucleoside triphosphate hydrolase	26 ancient paralogues on Ensembl (2022)
FGRAMPH1_01T07953	0.84	0.00	0.75	0.00	0.88	0.00	Folylpolyglutamate synthetase;Mur-like, catalytic domain	2 paralogues on Ensembl (2022)

superfamily;Mur ligase, C-terminal
domain superfamily

1315

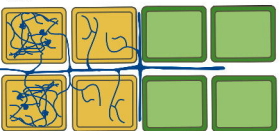
A

Stage

A B C D

Wheat Modules

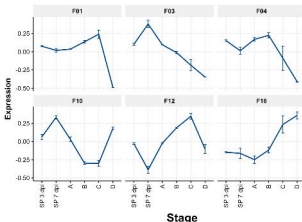
W02, W03, W02, W08, W12 W01, W05,
W06, W10, W12 W06, W22
W22



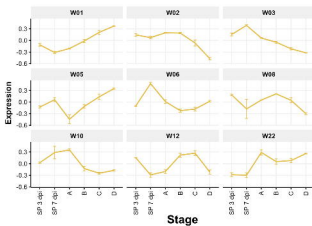
Fungal Modules

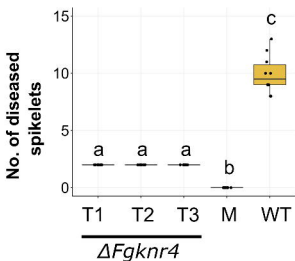
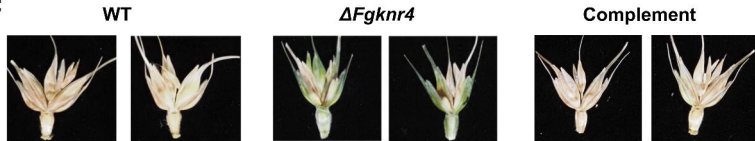
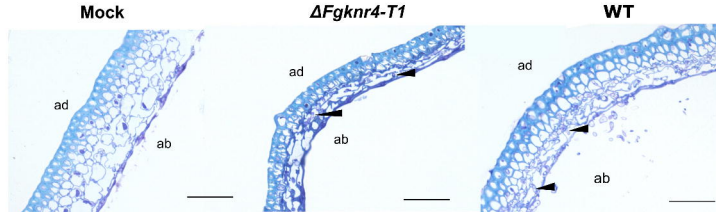
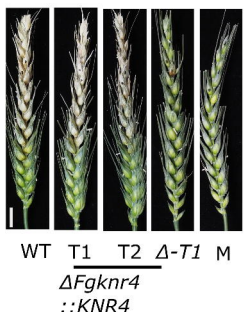
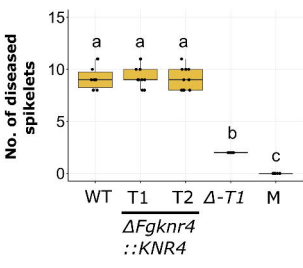
F03, F10 F01, F04 F01, F12 F10, F16

B

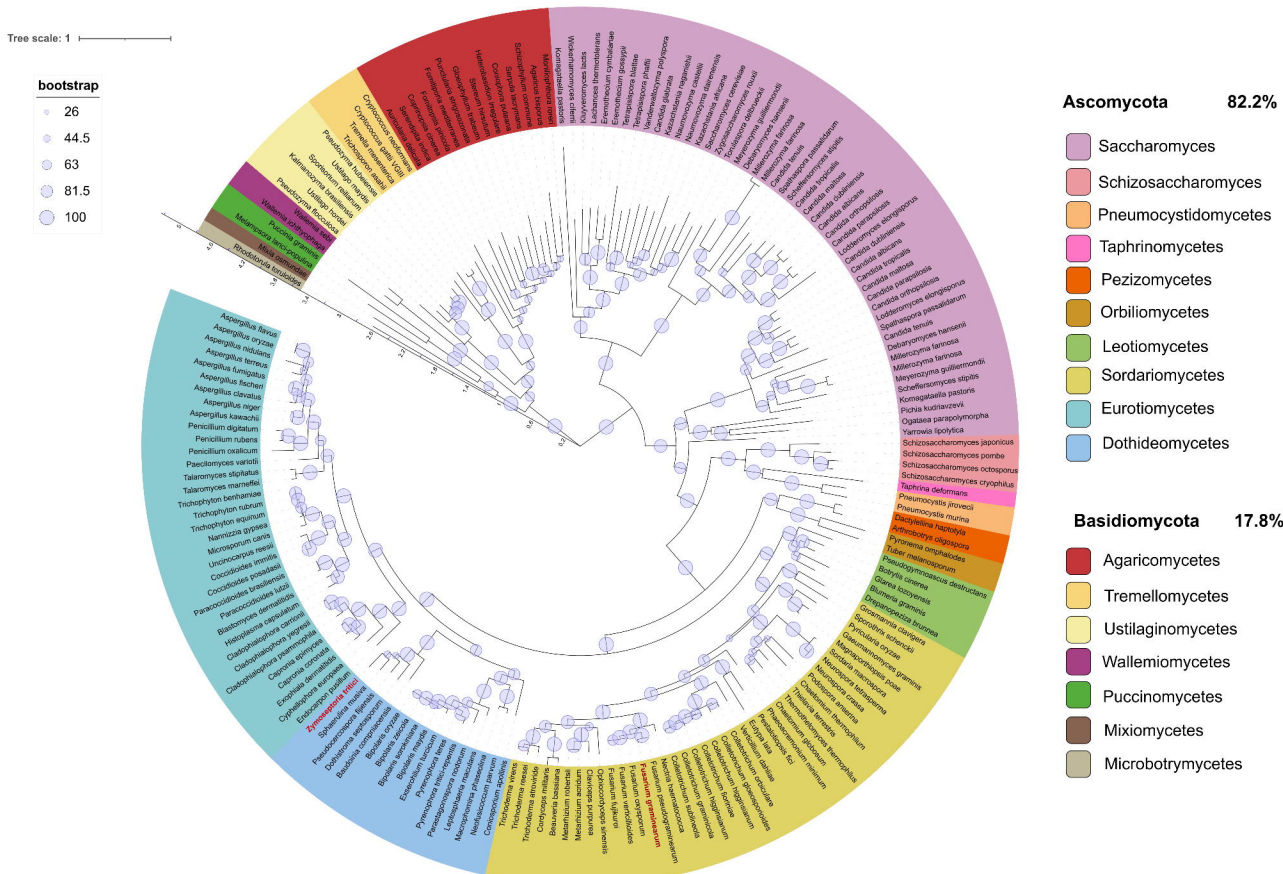


6



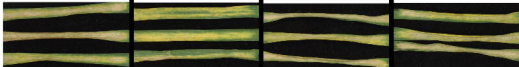
A**B****C****D****E****F**

Tree scale: 1



A

WT (IPO323)

 $\Delta Zt knr4$ $\Delta Zt knr4$
::KNR4-T1 $\Delta Zt knr4$
::KNR4-T2**B**

1 2 3

1 2 3

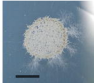
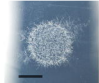
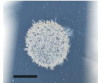
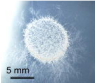
1 2 3

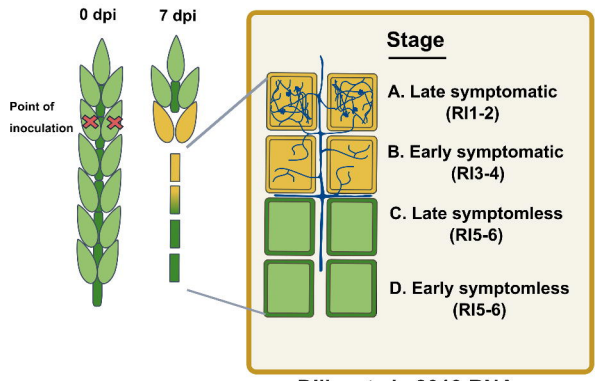
1 2 3

YPD

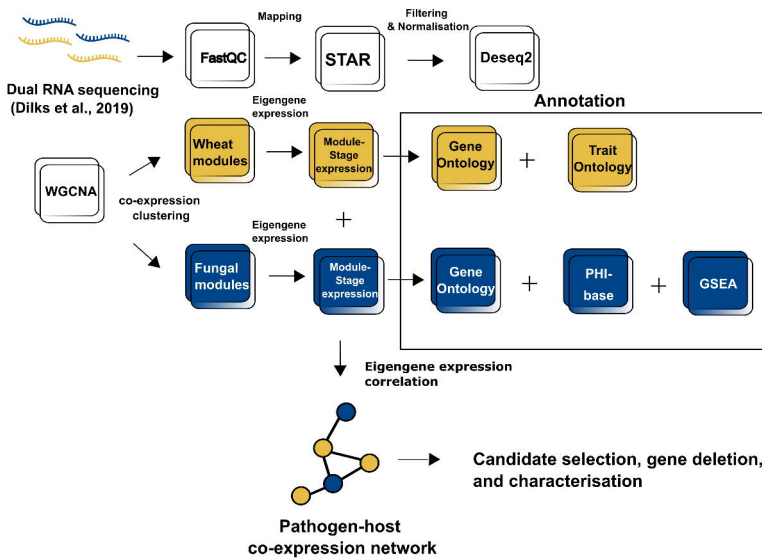


YPD+

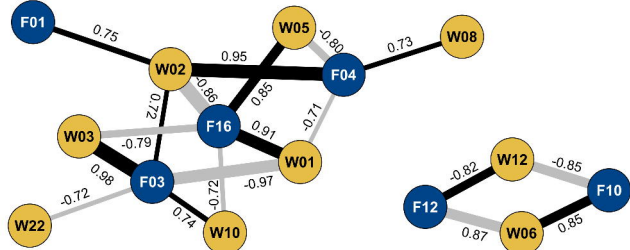
**C**

A

Dilks et al., 2019 RNA-seq

B

A



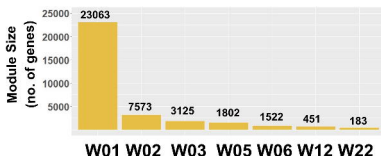
B



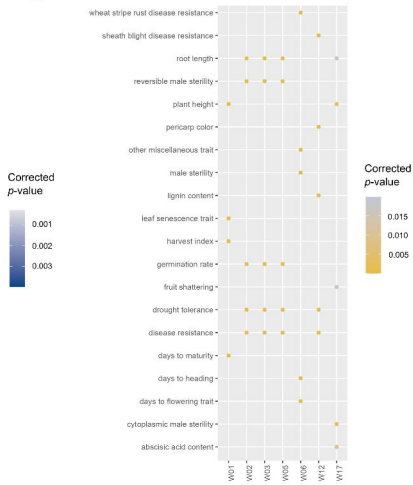
□

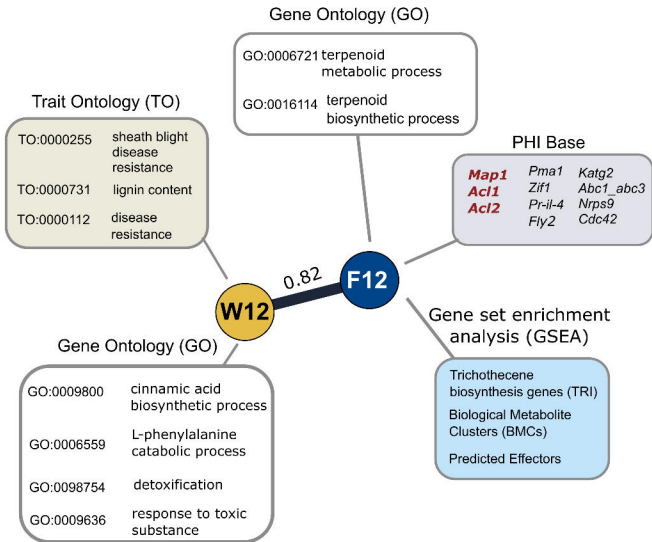
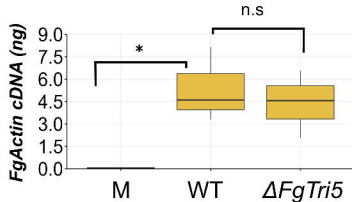
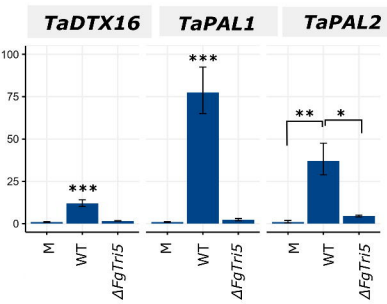


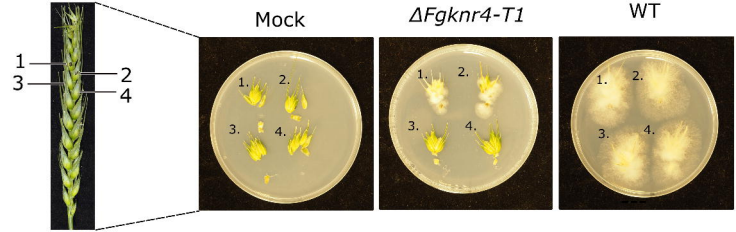
6

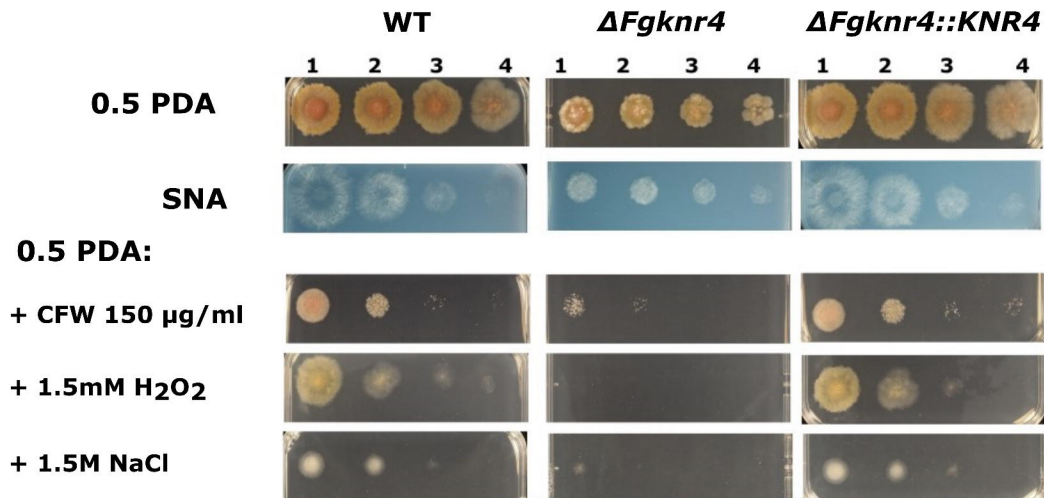
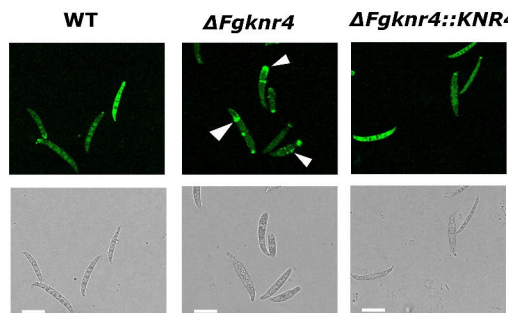
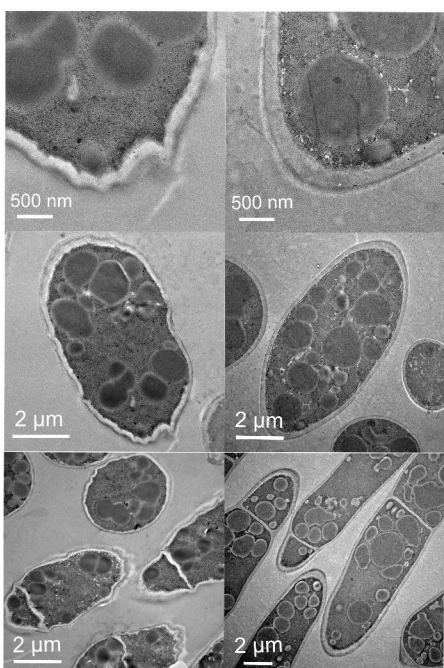
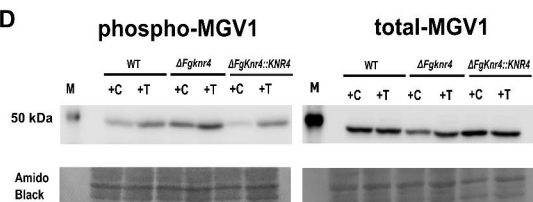


E

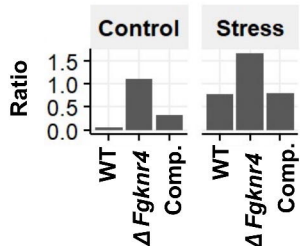


A**B****C**



A**B****C****D**Legend: **M** Marker, **C** Control (Water), **T** Treatment (200 μ g/ml CFW)**E**

Phosphorylated MGV1:Total MGV1

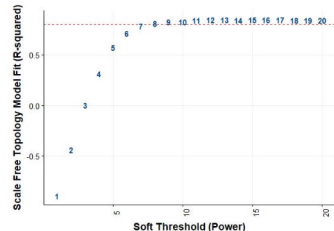


Module	Module Size	GO MF/BP Summary		GO CC Summary		Trait Ontology (TO)	
		BP	MF	BP	MF	TO	TO
25	83	DNA integration		Cell periphery		ethylene sensitivity	
24	96	Isopentenyl diphosphate biosynthesis		-		callus induction	
23	153	Protein modification		-		other miscellaneous trait	
22	183	-		-		other miscellaneous trait	
21	199	-		-		total root number	
20	235	DNA packaging		Nucleosome		cytoplasmic male sterility	
19	254	Lipid biosynthesis and protease activity		Lipid droplet		cytoplasmic male sterility	
18	287	Ubiquitination and protein catabolism		Proteosome complex		auxin sensitivity	
17	316	Diterpenoid biosynthesis		Extracellular region		cytoplasmic male sterility	
16	332	Protein phosphorylation and kinase activity		Integral component of membrane		disease resistance	
15	334	Fatty acid metabolism and synthesis				plant height	
14	374	Translation		Cytosolic ribosome		stem elongation	
13	379	Structural constituent of ribosome		Cytosolic ribosome		leaf senescence trait	
12	451	Detoxification and response to toxic substance		-		sheath blight disease resistance	
11	501	Glycolysis		-		self-incompatibility	
10	695	Protein localisation and autophagy		Protein-containing complex		male sterility	
9	765	Protein phosphorylation and kinase activity		Integral component of membrane		germination rate	
8	818	Protein phosphorylation and defense response		Integral component of membrane		disease resistance	
7	1544	Response to water and water channel activity		Chloroplast		cold tolerance	
6	1552	Protein catabolism and autophagy		Proteasome complex		days to flowering trait	
5	1802	Vesicle transport and hydrolase activity		Vesicle		disease resistance	
4	2344	Gene expression		Ribonucleoprotein complex		disease resistance	
3	3125	Proteolysis and autophagy		Peroxisome		disease resistance	
2	7573	Glutathione metabolism and response to biotic stimuli		Extracellular region		disease resistance	
1	23063	RNA modification and defense response		Chloroplast		harvest index	

Module	Module size	Phenotype				GO MF/BP Summary		GO CC Summary		Gene set enrichment				
		LOP	RV	L	U	BP	MF	BP	MF	TRI Genes	BMCs	Protein Kinases	Transcription Factors	Predicted Effectors
18	60	0	0	0	3			-						
17	62	0	0	0	3			-						
16	74	0	4	0	2			-						
15	75	0	0	0	2			-						
14	79	0	2	1	3			-						
13	121	0	2	0	6			-						
12	124	3	11	0	6	Terpenoid metabolic process		Extracellular region						
11	253	0	6	1	15			-						
10	275	0	11	0	14			-						
9	353	1	13	5	25			-						
8	406	0	10	1	9			-						
7	442	0	0	0	1	Translation		Cytoplasm						
6	607	0	9	3	35			-						
5	647	2	43	13	26	Metabolic processes		Cytoplasm						
4	1217	1	9	6	88	Transcription factor activity		Ribosome						
3	1278	0	6	1	77	Oxidoreductase activity		Membrane						
2	1487	4	66	12	88	Cellular Organisation		Membrane						
1	2629	4	65	16	184	Transcription factor activity		Nucleus						

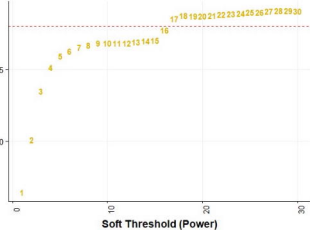
Fungal

A. Scale Free Model Fit (R-squared)

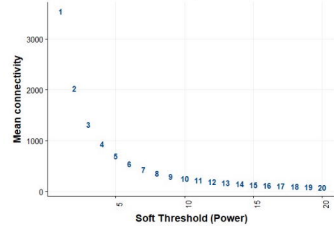


Wheat

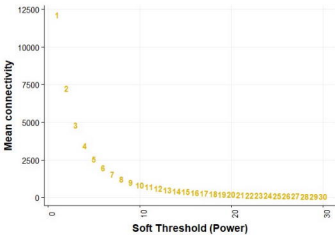
Scale Free Topology Model Fit (R-squared)



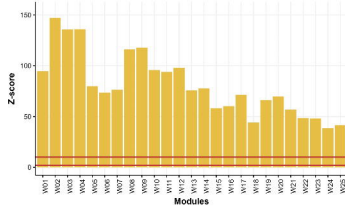
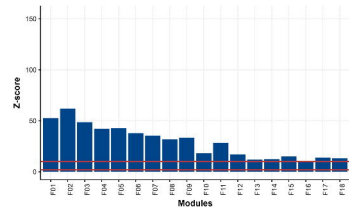
B. Mean Connectivity



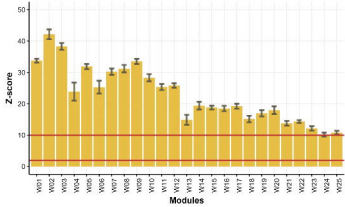
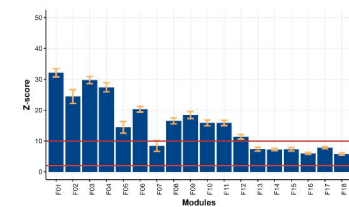
Mean connectivity



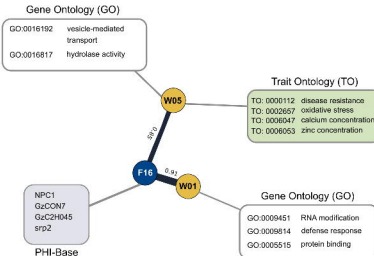
C. Module Quality



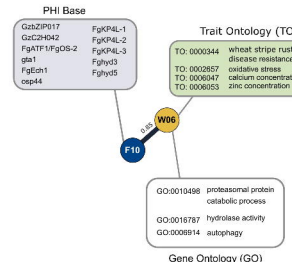
D. Module Preservation



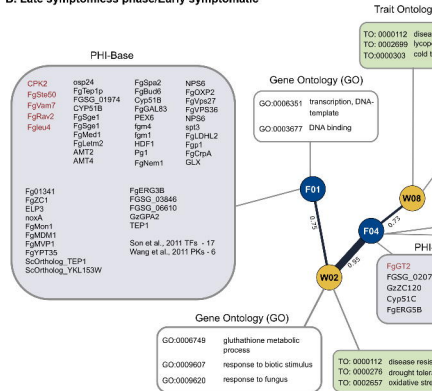
A. Early symptomless phase



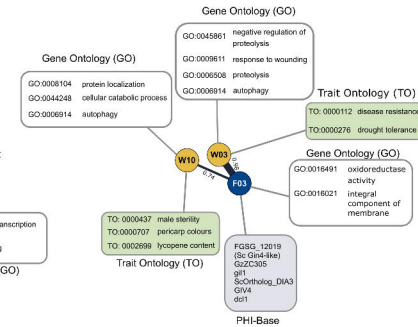
B. Early symptomless and late symptomatic

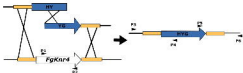
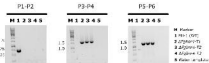
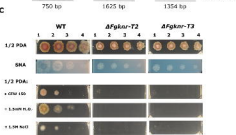


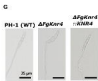
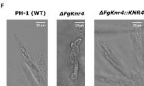
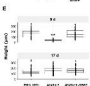
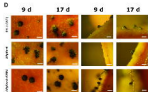
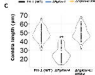
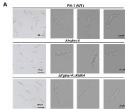
B. Late symptomless phase/Early symptomatic

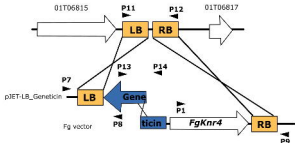
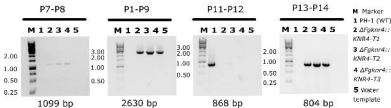
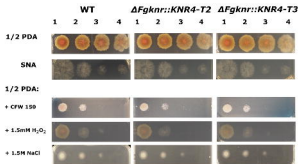


C. Late symptomatic phase



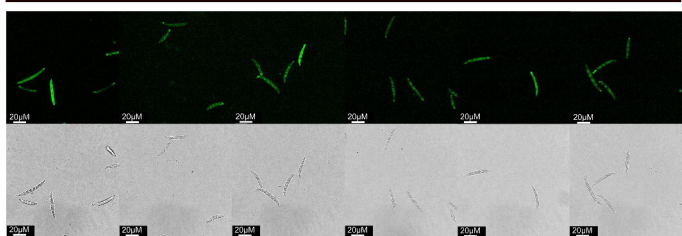
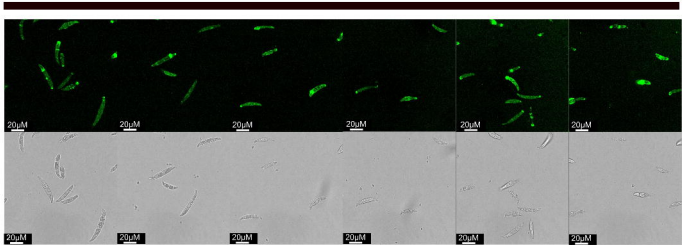
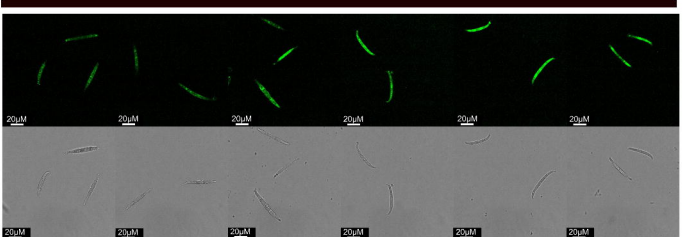
A**B****C**



A**B****C**

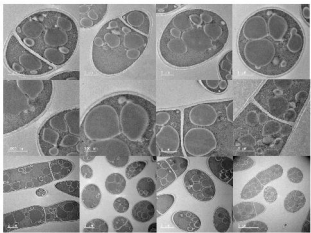
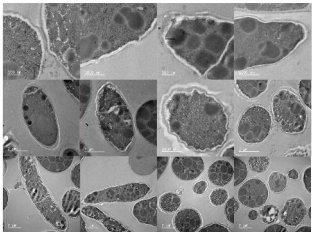
A

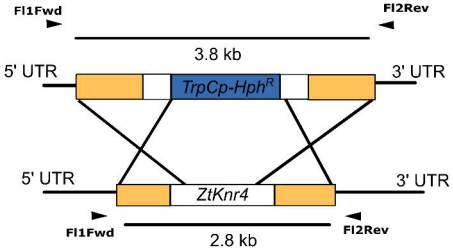
WT (PH-1)

**B** $\Delta Fgknr4 - T1$ **C** $\Delta Fgknr4::KNR4-T1$ 

A

WT (PH1)

**B** $\Delta Fgknr4 - T1$ 

A**B**